Geophys. J. Int. (2001) **144,** 271–288

Mantle convection with strong subduction zones

Clinton P. Conrad* and Bradford H. Hager

Department of Earth, Atmospheric, and Planetary Sciences, Massachusetts Institute of Technology, Cambridge, MA 02139, *USA*

Accepted 2000 August 18. Received 2000 August 2; in original form 2000 January 3

SUMMARY

Because mantle viscosity is temperature-dependent, cold subducting lithosphere should be strong, which implies that the rapid, localized deformation associated with subduction should strongly resist plate motions. Due to computational constraints, the deformation of a subducting plate cannot be accurately resolved in mantle-scale convection models, so its effect on convection is difficult to investigate. We have developed a new method for implementing subduction that parametrizes the deformation of the oceanic lithosphere within a small region of a finite element grid. By imposing velocity boundary conditions in the vicinity of the subduction zone, we enforce a geometry for subduction, producing a slab with a realistic thermal structure. To make the model dynamically consistent, we specify a rate for subduction that balances the energy budget for convection, which includes an expression for the energy needed to deform the oceanic lithosphere as it subducts. This expression is determined here from a local model of bending for a strong viscous lithosphere. By implementing subduction in this way, we have demonstrated convection with plates and slabs that resemble those observed on Earth, but in which up to 40 per cent of the mantle's total convective resistance is associated with deformation occurring within the subduction zone. This additional resistance slows plate velocities by nearly a factor of two compared to models with a weak slab. For sufficiently strong lithosphere, the bending deformation slows surface plates sufficiently that they no longer actively participate in global-scale convection, which occurs instead beneath a 'sluggish lid'. By introducing a low-viscosity asthenosphere beneath the oceanic plate, we demonstrate that small-scale convection at the base of oceanic lithosphere may limit plate thickness, and thus the resistance to bending, and cause plate velocities to depend on the strength of the bending lithosphere rather than on the viscosity of the underlying mantle. For a cooling Earth, the effective lithosphere viscosity should be nearly constant, but the mantle viscosity should increase with time. Thus, subduction-resisted convection should produce nearly constant plate velocities and heat flow over time, which has implications for the Earth's thermal evolution. We estimate that this style of convection should apply if the effective viscosity of the bending lithosphere is greater than about 10^{23} Pa s, but only if some mechanism, such as small-scale convection, prevents the bending resistance from stopping plates altogether. Such a mechanism could be fundamental to plate tectonics and Earth's thermal history.

Key words: lithosphere, mantle convection, plate tectonics, subduction, viscosity.

INTRODUCTION

The motions of Earth's tectonic plates are understood to be the surface expression of convection in the mantle. Because the plates are cold, they are denser than the mantle beneath them, and thus gravitationally unstable. For Earth, this instability manifests itself as subduction, in which oceanic lithosphere bends and dives into the mantle beneath overriding plates. Because it involves the entire oceanic lithosphere, subduction is an efficient mechanism for converting the significant negative buoyancy of the surface plates into horizontal density gradients that drive convection. In fact, subducted lithosphere is thought to drive plate motions, and thus mantle-scale flow, by pulling on attached surface plates (e.g. Chapple & Tullis 1977; Forsyth & Uyeda 1975; Hager & O'Connell 1981; Lithgow-Bertelloni & Richards 1995).

The cold temperatures of surface plates also make them stiffer than the underlying mantle, a fact that causes plates to move rigidly as coherent units. The temperature-dependent

* Now at: Seismological Laboratory, California Institute of Technology, Pasadena, CA 91125, USA. E-mail: clint@gps.caltech.edu

viscosity that strengthens plate interiors, however, should also strengthen subducting lithosphere, and thus tend to resist the rapid localized deformation associated with subduction. Indeed, numerical studies of mantle convection show that if temperature-induced viscosity contrasts are above 10^2–10^3, surface plates are slowed enough that they cannot actively participate in global-scale convective flow, which occurs instead beneath a 'sluggish lid' (e.g. Ratcliff *et al.* 1997; Solomatov & Moresi 1996). If viscosity contrasts reach 10^4–10^5, the boundary layer resists deformation altogether, forcing convection to occur beneath a 'stagnant lid' (e.g. Christensen 1984, 1985; Davaille & Jaupart 1993; Moresi & Solomatov 1995; Ratcliff *et al.* 1997; Solomatov 1995; Solomatov & Moresi 1996). Laboratory measurements of the temperature dependence of diffusion or dislocation creep in mantle rocks (e.g. Hirth & Kohlstedt 1996; Karato *et al.* 1986) suggest an order of magnitude variation in viscosity for every 100 °C of temperature change. For a temperature difference of ~600 °C across the ductile part of the lithosphere, viscosity variations should be more than sufficient for a stagnant lid to develop, yet this style of convection is not dominant for Earth. Subduction zones, then, serve to break an otherwise sluggish or stagnant lid by permitting the rapid localized deformation that is required for plate-like motions to occur. The weakening mechanism that allows subduction is not well understood, but brittle fracture (e.g. Moresi & Solomatov 1998; Zhong & Gurnis 1996; Zhong *et al.* 1998), strain-rate weakening (e.g. Tackley 1998), a maximum yield stress (e.g. Trompert & Hansen 1998), and various self-lubricating rheologies (e.g. Bercovici 1996, 1998; Lenardic & Kaula 1994) have been proposed as possibilities.

Generating plate-like behaviour in numerical models of mantle convection generally involves weakening convergent plate boundaries in some way, and justifying this action by appealing to one or more of the above mechanisms for weakening. For example, one commonly used method is simply to parametrize all of the possible weakening effects into low-viscosity 'weak zones' that are imposed between high-viscosity plates (e.g. Davies 1989; Gurnis & Hager 1988; King & Hager 1990, 1994; Puster *et al.* 1995). Weak zones can also be generated naturally by applying stress-weakening or self-lubricating constitutive laws to the lithosphere. This generates 'instantaneous' zones of weakness between rigid plates and avoids the necessity of imposing plate boundary locations (e.g. Bercovici 1996, 1998; Lenardic & Kaula 1994; Tackley 1998; Trompert & Hansen 1998). Other studies break strong lithosphere with weak faults that allow a jump in velocity across their width and that support some degree of shear stress (e.g. Toth & Gurnis 1998; Zhong & Gurnis 1994, 1995a,b; Zhong *et al.* 1998). Finally, plate-like behaviour can be forced by simply imposing piecewise continuous plate velocities at the surface (e.g. Hager & O'Connell 1979; Davies 1988; Bunge & Richards 1996). Such kinematic models avoid the difficulties of implementing realistic subduction zones, but are not dynamically self-consistent.

Due to computational constraints, the deformation associated with convergent plate boundaries typically spans only a few elements of a regularly spaced finite element grid. Thus, for the above methods to be accurate, they must include the deformation of a subducting plate within the small region of weakening in which subduction is implemented. It is not clear, however, that any of these studies achieve an accurate representation of subduction because the deformation that occurs in these studies is not compared to the deformation that can be observed at subduction zones. For example, the seismicity of the upper 200 km of Wadati–Benioff zones is thought to indicate plate bending as a slab begins to subduct, followed by unbending as it straightens and continues into the mantle (e.g. Bevis 1986, 1988; Engdahl & Scholz 1977; Hasegawa *et al.* 1994; Isacks & Barazangi 1977; Kawakatsu 1986). This unique strain pattern has been reproduced in detailed local models of subduction (e.g. Conrad & Hager 1999a; Houseman & Gubbins 1997; Melosh & Raefsky 1980; Toth & Gurnis 1998; Zhang *et al.* 1985) in which a strong plate is forced to bend as it passes through a realistic subduction zone geometry. Global-scale models must parametrize subduction more coarsely and thus cannot accurately compute the stresses associated with bending or unbending within the subducting plate.

If the deformation associated with subduction can be accommodated by a slab's elasticity, the net energy required to bend and then straighten the slab would be zero. Completely elastic bending, however, requires, that a plate be capable of supporting bending stresses of the order of 5000 MPa if an elastic plate thickness of 30 km and a bending radius of curvature of 200 km are assumed (e.g. Conrad & Hager 1999a; Isacks & Barazangi 1977). This is stronger than the maximum strength of oceanic lithosphere by about an order of magnitude (Kohlstedt *et al.* 1995). Instead, such stresses are likely to be relaxed by inelastic deformation mechanisms that dissipate energy and cause permanent deformation of the slab. One such inelastic deformation mechanism that dissipates energy as a plate bends and unbends is brittle fracture, which is expressed as seismicity within the slab (e.g. Chapple & Forsyth 1979). In addition, the mantle certainly behaves as a highly temperature-dependent fluid, so additional inelastic deformation should occur as viscous flow. Thus, subduction zones may demand a significant fraction of the mantle's total energy budget. In fact, Conrad & Hager (1999a) showed that if slabs remain two orders of magnitude stronger than the upper mantle as they descend, the bending and unbending of oceanic lithosphere at subduction zones may require as much energy as viscous flow within the mantle interior. If the energy spent on plate bending were available instead for deforming the mantle, as it would be if subduction zones were weak, significantly faster plate velocities would result. Thus, it is possible that plate bending at subduction zones, by retarding the flow of the oceanic lithosphere into the mantle interior, could limit plate velocities. This result was confirmed by Becker *et al.* (1999), who compared laboratory and numerical experiments for a growing slab.

Large-scale convection models that implement subduction by employing weak convergent plate boundaries do not permit significant energy to be dissipated at these boundaries. On the other hand, Conrad & Hager's (1999a) local model of subduction produces plate-like behaviour while dissipating significant energy within a subducting slab that remains strong as it deforms. Conrad & Hager's (1999a) subduction model, however, uses an irregular finite element grid that is both too complicated and of too high resolution to be of practical use in larger, mantle-scale studies. In this work, we devise a method for including the results of Conrad & Hager's (1999a) analysis within a small region of a large, regularly spaced, finite element grid. To do this, we impose a geometry for subduction that produces realistic temperature and velocity fields for the resulting slab. To make subduction dynamically self-consistent, we also specify the rate at which subduction occurs by applying Conrad & Hager's (1999a) energy balance analysis. This method

allows us to control how much energy is dissipated within the subduction zone, and thus parametrizes the effects of deformation within the subduction zone on convection in the entire mantle. Using this method, we study mantle convection with subduction zones that dissipate a significant fraction of the mantle's convective energy, as they should if oceanic plates remain strong as they subduct. In doing so, we determine the maximum amount of bending dissipation that is possible before 'sluggish lid' convection develops. In addition, we confirm some of the predictions made by Conrad & Hager (1999b), who suggested that the bending resistance at subduction zones could profoundly influence the Earth's thermal history.

THE ENERGETICS OF MANTLE AND LITHOSPHERE DEFORMATION

Convection in the mantle is typically formulated as a balance between gradients in viscous stresses and gravitational body forces, but it can also be described by an energy balance between the rate at which gravitational potential energy is released and the rate at which this energy is dissipated viscously by the deformation of mantle and lithosphere materials (e.g. Backus 1975; Chandrasekhar 1961, pp. 12–14; Conrad & Hager 1999a; Hewitt *et al.* 1975; Solomatov 1995). For this study, we implement subduction-driven convection using both approaches; we use a force balance to determine viscous flow within the mantle and an energy balance to describe the effects of subduction zone deformation on the entire convecting system. More specifically, we use an expression for the energy required to bend subducting lithosphere to parametrize the gross effects of this deformation on convection, but without requiring sufficient grid resolution to describe plate bending accurately. To implement this energy balance, we must first determine the energy dissipated by a subducting slab and compare this to the total energy requirements of convection. Here we follow the analysis of Conrad & Hager (1999a), who assumed a viscous rheology for the bending lithosphere. The approach, however, is general and dissipation associated with other deformation mechanisms could be included, if desired.

Mantle convection is driven by lateral variations in the mantle's density field. Potential energy is released largely by the downward motion of cold slabs and the upward motion of hot plumes. Making the Boussinesq approximation, the total potential energy release, Φ^{pe}, can be written as

$$\Phi^{\mathrm{pe}} = \int_A \rho g \alpha T(x, z) v_z(x, z) dA \,, \tag{1}$$

where ρ is the reference density, g is the acceleration due to gravity, α is the thermal expansivity, T is the temperature and v_z is the vertical velocity (positive upwards). For 2-D flow, the total potential energy release is calculated by integrating over the entire area, A, of the convecting system, and is given per unit length perpendicular to the plane of flow. For flow driven by the negative buoyancy of slabs, Conrad & Hager (1999a) showed that this expression becomes

$$\Phi^{\mathrm{pe}} = \frac{\rho g \alpha (T_{\mathrm{int}} - T_{\mathrm{s}}) l_{\mathrm{s}} h_{\mathrm{s}}}{\sqrt{\pi}} v_{\mathrm{p}} \equiv C^{\mathrm{pe}} v_{\mathrm{p}} \,, \tag{2}$$

where T_{int} and T_{s} are the temperatures of the mantle interior and surface, h_{s} is the thickness of the slab as it subducts, l_{s} is the length of the subducted portion of the slab and v_{p} is the slab's downward velocity, which we assume is equal to the velocity of the attached surface plate. Here we define the quantity C^{pe}, which will prove useful later, to express the dependence of Φ^{pe} on everything except for v_{p}.

The release of potential energy is balanced by energy dissipation throughout the entire convecting system. For viscous flow, the viscous dissipation, Φ^{vd}, can be written as (e.g. Chandrasekhar 1961, pp. 12–14)

$$\Phi^{\mathrm{vd}} = \int_A \tau_{ij} \dot{\varepsilon}_{ij} dA = 2 \int_A \eta \dot{\varepsilon}_{ij} \dot{\varepsilon}_{ij} dA \,, \tag{3}$$

where the strain rate, $\dot{\varepsilon}_{ij}$, is given by

$$\dot{\varepsilon}_{ij} = \frac{1}{2} \left(\frac{\partial u_i}{\partial x_j} + \frac{\partial u_j}{\partial x_i} \right) \tag{4}$$

and is related to the deviatoric stress, τ_{ij}, by the constitutive relation, again for incompressible flow,

$$\tau_{ij} = 2 \eta \dot{\varepsilon}_{ij} \,, \tag{5}$$

which defines the effective viscosity, η, of the fluid. For mantle flow driven by the motion of a plate and a slab, each moving with speed v_{p}, the total viscous dissipation can be expressed using eq. (3) as

$$\Phi^{\mathrm{vd}}_{\mathrm{m}} = C_{\mathrm{m}} \eta_{\mathrm{m}} v_{\mathrm{p}}^2 \,, \tag{6}$$

where η_{m} is the effective mantle viscosity and C_{m} is a geometrical constant of the order of 10^0–10^1 that depends on the pattern of flow (Conrad & Hager 1999a).

Because their viscosity is temperature-dependent, subducting slabs should have a strength, expressed here as an effective viscosity η_{l}, that is greater than that of the underlying mantle. In addition, subduction zones accommodate large changes in velocity over short horizontal distances, which implies large strain rates. According to eq. (3), both of these facts indicate that the viscous dissipation for a subduction zone should be large. Solomatov (1995) suggested that the dissipation within a cold, strong boundary layer may, in certain cases, be comparable to the potential energy released by vertical motion of this boundary layer. By combining theory with numerical calculations, Conrad & Hager (1999a) showed that the bending and unbending of an effectively viscous lithosphere in a subduction zone produces a viscous dissipation, $\Phi^{\mathrm{vd}}_{\mathrm{l}}$, of

$$\Phi^{\mathrm{vd}}_{\mathrm{l}} = 2 v_{\mathrm{p}}^2 \eta_{\mathrm{l}} \left(\frac{h_{\mathrm{s}}}{R} \right)^3 \,, \tag{7}$$

where R is the radius of curvature that describes the bent shape of the slab. Conrad & Hager (1999a) showed that $\Phi^{\mathrm{vd}}_{\mathrm{l}}$ may be larger than $\Phi^{\mathrm{vd}}_{\mathrm{m}}$ if the effective lithosphere viscosity is of the order of 10^{23} Pa s, which is only about two orders of magnitude larger than estimates for the average viscosity of the mantle. Significant energy dissipation may also be associated with other aspects of the subduction zone. For example, Conrad & Hager (1999a) estimated that dissipation in the fault zone between the slab and the overriding plate may account for up to 10 per cent of the mantle's total energy dissipation. Additional dissipation may result from corner flow in the mantle associated with the motion of the subducting plate.

Below we assume that R, the bending radius of curvature, remains constant despite variations in the plate thickness, h_{s}. This assumption largely agrees with previous analyses of Benioff zone seismicity, which show that subduction under Alaska, the Aleutians, Kamchatka, Japan, New Zealand and Tonga all

exhibit a bending radius of curvature of about 200 km (Isacks & Barazangi 1977). The subducting plates in these regions range in age from less than 50 Ma (Alaskan and Aleutian subduction) to more than 100 Ma (the others) (Jarrard 1986), and thus represent a range of subducting plate thicknesses. Subducting plates can bend more sharply, as subduction under the New Hebrides and Central America shows (50 and 20 Ma respectively), or less sharply, as exemplified under South America and Cascadia (50–80 and 10 Ma respectively) (Isacks & Barazangi 1977; Jarrard 1986). If R and h_s were positively correlated, the plate thickness dependence of Φ_m^{vd} in eq. (7) would be diminished; the reverse would be true of they were negatively correlated. The above ages indicate that younger and thinner plates can display bending radii that are either larger or smaller than the approximate global average of 200 km, indicating that h_s and R are not correlated. Our assumption that R has a constant value of 200 km is consistent with this observation, but ignores the variations that are observed in R between subduction zones.

In addition, the effective lithosphere viscosity, η_l, that applies in eq. (7) represents the combined effects of all of the deformation mechanisms that contribute to bending of the lithosphere, which should include viscous flow, brittle fracture, non-Newtonian flow and plastic deformation. In using eq. (7) to express the bending dissipation, an assumption is made that η_l does not vary with either the plate velocity v_p or the plate thickness h_s. If, however, the viscosity depends on stress or strain rate, then η_l should decrease as either of these quantities increase. In the limit that the lithosphere's brittle rheology causes it to fail for stresses above some maximum yield stress, eq. (3) suggests that Φ_l^{vd} should be linearly dependent on v_p. Similarly, bending stresses should increase as h_s increases, implying that stress-weakening should cause the effective viscosity η_l to be smaller for thicker plates. In this analysis, we study how one model for subduction zone deformation affects mantle-scale convection, using eq. (7) to express bending for a viscous lithosphere. We recognize that non-linear viscosity or subduction zone deformation not associated with bending may introduce additional behaviour, but save the analysis of such behaviour for future study.

INCLUDING PLATE BENDING WITHIN A NUMERICAL CONVECTION SIMULATION

To simulate the bending of oceanic lithosphere in a subduction zone, we modify ConMan, a finite element code that solves the coupled thermal diffusion and incompressible Navier–Stokes equations for a highly viscous fluid (King *et al.* 1990). These modifications allow the effects of plate bending to be included within a small region of a regular finite element grid. To illustrate this, we set up a finite element grid (Fig. 1) with aspect ratio 2.5, a resolution of 40 by 100 elements, free-slip boundary conditions on the bottom surface and periodic boundary conditions on the two sides. Boundary conditions at the top surface are a mixture of free slip, representing a mobile oceanic plate, and no slip, representing a continental plate. Temperature boundary conditions maintain constant temperatures T_b at the grid base and $T_s < T_b$ at the surface and, coupled with a non-zero thermal diffusivity, κ, cause thermal boundary layers to form at these boundaries. Temperature-dependent viscosity

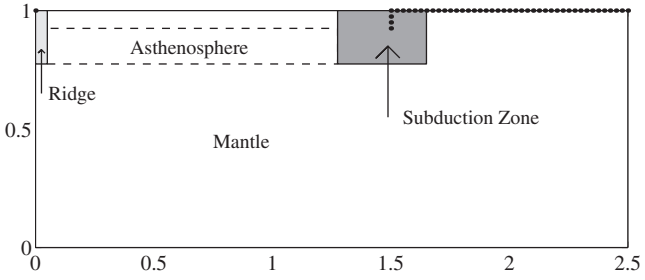

Figure 1. Cartoon showing the various regions of the finite element grid. Viscosity is temperature-dependent, but weaker by a factor of 10 within the ridge and the asthenosphere, which is not included in all calculations. Zero-velocity boundary conditions (dots) on the surface, combined with the temperature-dependent viscosity, allow the formation of a high-viscosity continental plate. The oceanic plate between the ridge and the subduction zone is mobile and is forced into the mantle interior at the subduction zone, where a set of specially designed velocity boundary conditions (detailed in Fig. 2) impose the geometry for subduction.

makes the oceanic lithosphere strong and thus causes its motions to be plate-like. The oceanic lithosphere is bounded on one side by a low-viscosity 'ridge' and on the other side by a specially designed 'subduction zone' that implements the descent of oceanic lithosphere into the mantle and expresses the energy requirements of a bending plate, as described below. The negative buoyancy of this subducted slab largely drives convective flow, both for this bottom-heated model and in the Earth's mantle, which is partially heated internally. Because in thermal steady state the boundary layer for both cases should be nearly identical, convection rates for both cases should be similar, and the results presented here should apply equally.

Non-dimensionalization

At this point, it is useful to define a set of dimensionless variables. We define the Rayleigh number, Ra_m, for the convecting system as

$$Ra_m = \frac{\rho g \alpha \Delta T D^3}{\kappa \eta_m}, \tag{8}$$

where ΔT is the temperature difference $T_b - T_s$, D and κ are the thickness and thermal diffusivity of the mantle layer and η_m is its average viscosity, which in these calculations is calculated by following Parmentier *et al.* (1976), who suggest weighting the viscosity by the square of the strain rate because the viscosity in the more rapidly straining areas is more important to the total flow field. We define a dimensionless viscosity, η', as

$$\eta' = \frac{\eta}{\eta_0}, \tag{9}$$

where η_0 is the mantle viscosity corresponding to $Ra_m = 10^6$, a value we use as a reference value in the calculations to follow. In these calculations, we vary Ra_m by changing η_m, keeping the other terms in the Rayleigh number, as defined by eq. (8), constant. We define a dimensionless temperature, T', according to

$$T' = \frac{T - T_s}{T_b - T_s}. \tag{10}$$

Thus, $T'=0$ at the surface and $T'=1$ at the base. Finally, we non-dimensionalize time and distance according to

$$t'=t\,\frac{\kappa}{D^2} \qquad \text{and} \qquad x'=\frac{x}{D}\,, \tag{11}$$

which implies a non-dimensionalization for velocity of

$$v'=v\,\frac{D}{\kappa}\,. \tag{12}$$

Viscosity structure

To generate a strong plate at the surface, we impose temperature-dependent viscosity using the viscosity law (e.g. Kohlstedt *et al.* 1995),

$$\eta'_{\rm m}(T')=\eta'_{\rm m}(T'_{\rm int})\exp\left(\frac{E_{\rm a}}{RT'\Delta T}-\frac{E_{\rm a}}{RT'_{\rm int}\Delta T}\right), \tag{13}$$

where $E_{\rm a}$ is an activation energy, $R=8.31$ J mol^{-1} K^{-1} is the universal gas constant and we assume a non-adiabatic temperature variation between $T_{\rm s}=0$ °C at the surface and $T_{\rm b}=2000$ °C at the base. We choose an initial interior temperature of $T_{\rm int}=1300$ °C, which is a reasonable value for the Earth (e.g. Turcotte & Schubert 1982, p. 192). This corresponds to a dimensionless value of $T'_{\rm int}=0.65$, which is close to the steady-state interior temperatures that are produced in this study. We choose an activation energy of $E_{\rm a}=100$ kJ mol^{-1} because this value is large enough to produce plates and slabs that move as coherent units, but small enough to prevent the entire mantle from evolving into a cold, immobile state. The value of $\eta'_{\rm m}(T'_{\rm int})$ is varied to produce different mantle Rayleigh numbers, $Ra_{\rm m}$. Finally, we set a maximum viscosity of $\eta'_{\rm max}=1000$ for all runs. This clips the extremely large viscosities inherent in eq. (13) as $T'\to 0$ but also maintains a constant high viscosity at the surface that is not dependent on the interior viscosity. This feature is useful in an application to the thermal evolution of the Earth.

The 'ridge' is a region two elements wide and nine deep that has a temperature-dependent viscosity of $\eta'_{\rm r}(T')=0.1\eta'_{\rm m}(T')$. The weakness of the ridge allows the oceanic plate to pull away from the continent easily. Later, we include a low-viscosity asthenosphere beneath the oceanic plate by applying a temperature-dependent viscosity of $\eta'_{\rm as}(T')=0.1\eta'_{\rm m}(T')$ to the fourth–ninth elements from the surface, between the ridge and the subduction zone.

The subduction zone

To implement subduction, we apply velocity boundary conditions within, and on the boundaries of, the subduction zone region (Fig. 2). On the left-hand edge of the subduction zone, an imposed horizontal velocity of magnitude v_i forces the oceanic plate into the subduction zone. This material is later forced vertically out of the bottom of the subduction zone region with a downward speed of v_i. Within the subduction zone, the fluid is forced to turn smoothly by velocity boundary conditions, also of magnitude v_i, directed tangentially to an arc with radius of curvature equal to $R'=0.225$, which is the depth of the subduction zone region. Other boundary conditions include free slip along the top surface and pinned nodes along the boundary with the overriding plate (Fig. 2). By imposing

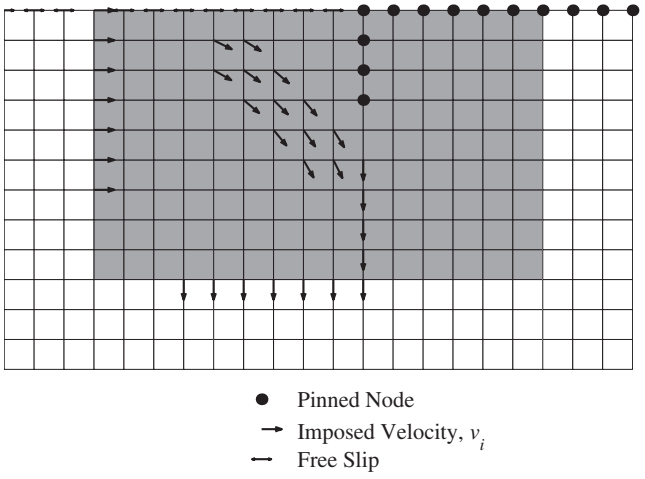

Figure 2. A detail of the subduction zone region of the finite element grid showing the velocity boundary conditions used to implement subduction. The large dots indicate pinned nodes and double-sided arrows indicate free-slip boundaries. Large arrows indicate the direction of the imposed velocity boundary conditions, which force subduction with a realistic geometry and produce a realistic thermal structure for the resulting slab. All of the imposed velocities have the same magnitude v_i, which is determined by the iterative procedure described in the text. This procedure balances potential energy release with the energy dissipated viscously, which, for the shaded region, is explicitly defined using a model for the energy dissipation associated with subduction zone deformation.

vertical flow along the boundary with the lower continent, we direct flow within the subduction zone and also draw hot fluid from the mantle into the region adjacent to the subduction zone, preventing cold material from accumulating there. This set of boundary conditions for the subduction zone generates stable subduction that can be implemented indefinitely, as long as the thickness of the thermal boundary layer does not exceed that of the subduction zone region.

We must choose the speed, v_i, with which we force subduction to occur. Because the oceanic plate is strong, forcing subduction at a speed v_i causes the plate velocity, $v_{\rm p}$, to be equal to v_i. To generate convection that is fully dynamic but that still includes the proper amount of dissipation within the subduction zone, we require the total energy dissipated to be equal to the total potential energy released. Thus, we choose v_i so that $\Phi^{\rm pe}=\Phi^{\rm vd}_{\rm m}+\Phi^{\rm vd}_{\rm l}$, which, using eqs (2), (6) and (7) gives

$$v_{\rm p}=v_i=\frac{C^{\rm pe}}{C_{\rm m}\eta_{\rm m}+2\eta_{\rm l}(h_{\rm s}/R)^3}\,. \tag{14}$$

The plate thickness, $h_{\rm s}$, is measured directly from the temperature profile of the slab, while the bending radius of curvature, R, and the lithosphere effective viscosity, $\eta'_{\rm l}$, are model parameters that are used only in the parametrization of plate bending in the subduction zone. Expression (14) gives the speed with which subduction must be driven in order for the subduction zone to dissipate the prescribed amount of energy. To use this expression, however, we must know $C_{\rm m}$ and $C^{\rm pe}$ for a potentially complicated flow pattern. Because the dependence of $C_{\rm m}$ and $C^{\rm pe}$ on $v_{\rm p}$ is weak, we can estimate these quantities by first forcing the system with a chosen velocity v_{i-1}, measuring $\Phi^{\rm vd}_{\rm m}$ and $\Phi^{\rm pe}$ using eqs (3) and (1) and then applying eqs (2) and

(6). In measuring Φ_m^{vd}, we exclude the dissipation that occurs within the subduction zone region (Figs 1 and 2) because we include an explicit expression for the dissipation associated with subduction in eq. (14). Applying these estimates for C_m and C^{pe} to eq. (14) yields a new expression for v_i that depends on v_{i-1}:

$$v_p = v_i = \frac{\Phi^{pe}/v_{i-1}}{\Phi_m^{vd}/v_{i-1}^2 + 2\eta_l (h_s/R)^3}. \quad (15)$$

Thus, the proper subduction rate can be calculated using an iterative procedure in which the effects of applying a speed v_{i-1} are tested by measuring Φ_m^{vd} and Φ^{pe} for this speed. A new speed v_i is then calculated using eq. (15) and then tested in the same manner. This procedure is repeated until the imposed speed does not change by more than 0.01 per cent. The resulting value of v_i is the rate for subduction that balances potential energy release and the total viscous dissipation, which includes the contribution from the bending slab. This subduction rate is used to advance the flow field by a single time step, and is then used as the initial test velocity for the next time step. If the flow field is close to steady state, convergence occurs in only a few iterations. If the flow field is changing rapidly, convergence typically requires 10–20 iterations.

This iteration procedure produces a flow field for which the total potential energy release is equal to the sum of the measured viscous dissipation for the mantle and an externally specified expression for the viscous dissipation associated with bending a viscous slab. Thus, it includes, in a dynamically consistent way, the bending deformation of a potentially strong viscous plate, without requiring the grid resolution necessary to model this deformation accurately. The accuracy of the implementation instead depends on the accuracy of Φ^{pe} and Φ_m^{vd}. We can estimate the error associated with calculating these quantities by comparing Φ^{pe} and Φ^{vd} for a run in which we do not impose velocity boundary conditions, in which case we expect $\Phi^{vd} = \Phi^{pe}$. For the finite element grid that we use, we find that Φ^{pe} is typically greater than Φ^{vd} by up to 2 per cent for $Ra_m \sim 10^5$ and by up to 5 per cent for $Ra_m \sim 10^7$. This difference is associated with errors in the velocity field. Potential energy release depends linearly on velocity, as in eq. (1), whereas viscous dissipation depends on the square of gradients in velocity, as in eq. (3). Measurements of the latter should be less accurate because Φ^{vd} includes a gradient of the velocity term, and because this term is squared. This is indeed what we find in tests: measurements of Φ^{pe} converge more rapidly with increasing grid resolution than do measurements of Φ^{vd}. Because our measurements of Φ_m^{vd} are slightly too small, our method of forcing the viscous dissipation to balance the potential energy release causes too much viscous dissipation to be placed in the bending lithosphere. This overestimate could be up to 5 per cent for Rayleigh numbers close to 10^7, which are the least resolved of our calculations.

Implementation of the subduction zone

To implement this iteration procedure, we modified the finite element code ConMan (King *et al.* 1990), which calculates the flow velocity field by solving $\mathbf{Ku} = \mathbf{f}$ for $\mathbf{u}$, which is a vector of unknown velocities. Here $\mathbf{K}$ is the 'stiffness' matrix, which implements the equations of incompressible Stokes flow for the given finite element grid, and $\mathbf{f}$ is a vector that describes the buoyancy forces that drive the flow. The most time-consuming step in solving for $\mathbf{u}$ is inverting $\mathbf{K}$, an operation that must be performed at every time step if the viscosity field changes with time (as it does for temperature-dependent viscosity). Velocity boundary conditions are implemented by removing the specified velocities from $\mathbf{u}$, multiplying them by the associated columns of $\mathbf{K}$, and then moving the result to the right-hand side. For our application, this can be written as

$$\mathbf{K}_r \mathbf{u}_r = \mathbf{f} - \frac{v_i}{v_{i-1}} \sum_j u_j \mathbf{k}_j, \quad (16)$$

where u_j is the jth velocity boundary condition, $\mathbf{k}_j$ is the jth column of $\mathbf{K}$, the subscript r indicates that rows or columns have been removed, and the summation is over all of the imposed velocity boundary conditions. The factor v_i/v_{i-1} is a multiplicative factor that updates the velocity boundary conditions used to implement subduction for the ith iteration. Because this factor does not operate on the stiffness matrix $\mathbf{K}_r$, it is possible to update the imposed subduction velocity for each iteration without reinverting $\mathbf{K}_r$. As a result, the iteration procedure runs quickly and does not add prohibitively to the total computation time.

EXAMPLES OF CONVECTION WITH A BENDING LITHOSPHERE

To initiate subduction, we first impose a constant subduction velocity of $v_i' = 500$ on an initially isothermal mantle with temperature $T_{int}' = 0.65$ and Rayleigh number $Ra_m = 10^6$. The cold temperature boundary condition at the surface cools the fluid there and the resulting thermal boundary layer is subducted into the mantle interior, forming a slab. Once the temperature field ceases to change significantly with time, it is used as a starting point for runs in which the rate of subduction is dynamically chosen according to the method described above. For these calculations, an effective viscosity for the lithosphere, η_l', is chosen so that the viscous dissipation of the bending slab can be calculated from eq. (7). To calculate Φ_l^{vd}, we estimate the plate thickness, h_s', using the depth of the $T' = T_{int}'\,\mathrm{erf}(1) = 0.55$ isotherm. This isotherm was chosen because it represents a high temperature that is consistently within the boundary layer, and thus provides a reliable scale for the boundary layer thickness. As described above, we assume a bending radius of curvature of $R' = 0.225$. For each choice of lithosphere viscosity η_l', we allow dynamically driven subduction to proceed until the system has reached an approximate steady state. Because as each system evolves, the mantle typically warms slightly, the viscosity there decreases, leading to Rayleigh numbers greater than the initial value of 10^6.

As a first example, we apply an effective lithosphere viscosity of $\eta_l' = 500$. A snapshot of convection at thermal steady state (Fig. 3) features a flow field and a temperature structure that are consistent with rigid plate motions and subduction-dominated flow. This slab originates at the subduction zone (Fig. 3a), where the velocity boundary conditions generate subduction-like flow of the cold oceanic lithosphere into the underlying mantle (Fig. 3b). This flow is not entirely smooth because the imposed velocity boundary conditions are not optimized for incompressible flow. The extra energy dissipated

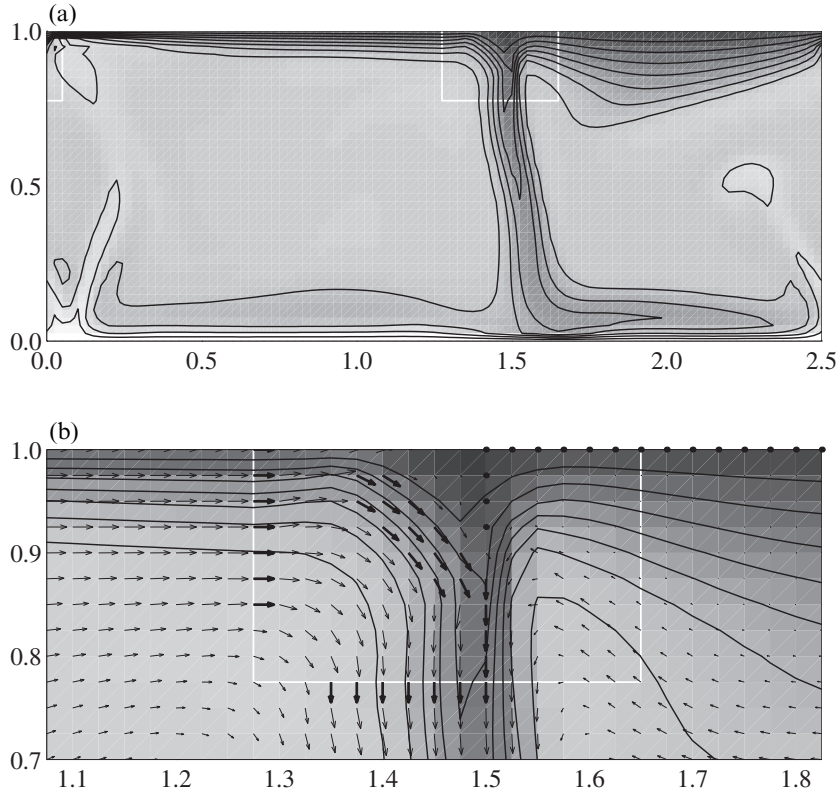

Figure 3. A snapshot of convection that includes a bending slab ($\eta_l' = 500$) and $Ra_m = 1.4 \times 10^6$. This combination leads to an average plate speed of $v_p' = 671$ and an average plate thickness of $h_s' = 0.066$. Here, because the slab is strong, 40 per cent of the total viscous dissipation is accounted for by plate bending within the subduction zone; the rest is dissipated viscously in the mantle. The subduction zone and ridge are outlined in white for reference. The temperature field is shown in (a), and is denoted by grey shading (colder is darker) and contours, where the contour interval is 10 per cent of the total temperature variation across the grid. Shown in (b) is a detail of the subduction zone and its surroundings, where the flow field is indicated by arrows. Thick arrows indicate imposed velocities that force fluid through the subduction zone.

by local irregularities in this flow field, however, has negligible effect because our method for implementing subduction replaces any energy dissipation that occurs within the subduction zone by eq. (7), an expression for this dissipation derived from a local study. The downgoing slab also draws hot mantle material to the region below the overriding plate (Fig. 3b). This flow is important because it prevents the development of an overly thick continent by constantly removing cold fluid from the continental base.

Even after the calculation has reached its 'steady state', quantities such as the plate velocity v_p' and the subducting plate thickness h_s' continue to change with time, oscillating about some mean value, as is shown for several different values of η_l' in Fig. 4. Short timescale variations in the driving buoyancy field, which occur as the slab interacts with the overriding plate or the base of the mantle, could cause this behaviour. In addition, slight variations in the measured value of the plate thickness, h_s, should have an amplified effect on plate velocity because the bending resistance depends on the cube of h_s, as in eq. (7).

For relatively weak lithosphere with $\eta_l' = 10$, an average of only 1 per cent of the total viscous dissipation occurs as parametrized plate bending within the subduction zone (Fig. 4c). Thus, for weak lithosphere, bending provides little resistance to convection and plate motions. Increasing the effective lithosphere viscosity to $\eta_l' = 100$ or $\eta_l' = 500$, however, causes the viscous dissipation associated with bending to increase (Fig. 4c), which leads to lower plate speeds (Fig. 4a). The slower plates are slightly thicker (Fig. 4b) because they have more time to cool as they travel from the ridge to the trench. For a bending slab with viscosity $\eta_l' = 500$, bending dissipation accounts for 40 per cent of the total (Fig. 3).

Increasing the plate viscosity still further to $\eta_l' = 1000$ slows the plate significantly (Fig. 4a), which causes it to thicken. The greater plate thickness increases the bending resistance because Φ_l^{vd} depends on the cube of the plate thickness, as shown by eq. (7), and thus leads to a further slowing of the plate. This runaway process rapidly decelerates the plate (Fig. 4a) and ultimately causes it to thicken by over a factor of two (Fig. 4b). Because the plate motion is so significantly slowed, the deformation occurring within the subduction zone becomes smaller compared to that occurring within the underlying mantle, as evidenced by the decreased average bending dissipation of 27 per cent (Fig. 4c). The temperature and flow fields at steady state (Fig. 5) show convection occurring primarily beneath a 'sluggish lid'. Although a downwelling in the vicinity of the subduction zone is still evident, it involves only the hottest few isotherms and consists of material moving at speeds that are much larger than those of the oceanic plate.

Thus, it appears that the total fraction of dissipation that can occur within the subduction zone may be limited. If the subduction zone is too strong, surface plates are slowed and thicken until 'sluggish lid' convection develops. We have generated plate-like motions, however, for convection in which $\sim$40 per

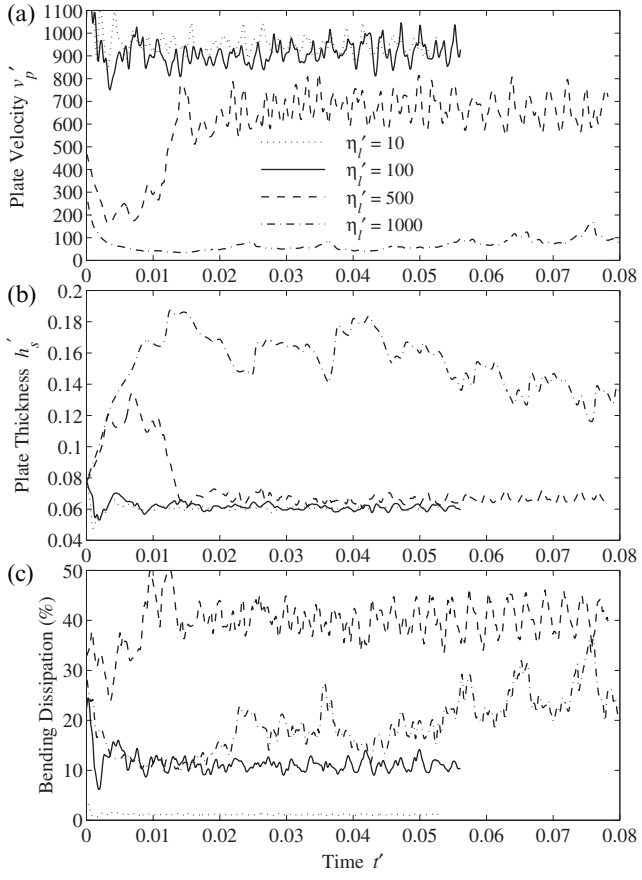

Figure 4. A comparison of (a) plate velocity v_p', (b) plate thickness h_s' and (c) the fraction of the total energy dissipation that occurs as plate bending within the subduction zone as a function of time. Results are shown for four subducting slabs with η_l' of 10, 100, 500 and 1000, for which Ra_m is 1.1×10^6, 1.1×10^6, 1.4×10^6 and 2.5×10^6.

cent of the total viscous dissipation occurs as plate bending within the subduction zone. This is a large fraction of the total and demonstrates that subduction zones could provide significant resistance to convection while still allowing mobile plates at the surface.

COMPARISON TO WEAK-ZONE SUBDUCTION MODELS

For the Earth, plate-scale downwelling is characterized by the entire thickness of an oceanic plate descending into the mantle interior beneath an overriding plate. Thus, subduction is an inherently asymmetrical process that includes simple shear along a plate-bounding fault. Here we implement subduction using a set of velocity boundary conditions that are designed to move the entire thickness of the thermal boundary layer efficiently into the fluid interior. Thus, we expect our method for implementing subduction to produce slabs with temperature profiles that resemble those expected for the Earth. Other methods that employ a simple 'weak zone' for implementing subduction result in pure shear deformation at the surface, which, as discussed below, changes the thermal structure of the downwelling that is produced.

To demonstrate this point, we compare our implementation of subduction to a pure shear implementation in which we implement a 'weak zone' by imposing a constant, but low, viscosity of $\eta_{wz}' = 1$ between the oceanic and continental plates. The resulting flow (Fig. 6a) features a mobile oceanic plate but a large area of cold fluid forms beneath the continent adjacent to the 'weak zone'. This mass of cold, stiff material develops because the pure shear deformation associated with the 'weak zone' generates a flow that draws fluid from beneath the continent, rather than from the mantle below. Because this fluid is cold, and therefore stiff, it accumulates there, forcing cold subducting material to descend around it, cooling it further. On the other hand, if velocity boundary conditions are used to implement subduction, hot fluid from the mantle is drawn upwards next to the subducting slab, preventing the accumulation of cold fluid there (Fig. 3). The amount of cold fluid that accumulates next to the slab can be diminished by decreasing the activation energy associated with the temperature dependence of viscosity. If, however, we decrease E_a to 50 kJ mol^{-1}, a more slab-like downwelling forms, but cold fluid still accumulates next to the slab (Fig. 6b). This value for E_a is equivalent to the value used by King & Hager (1994) in a similar calculation that also produces an accumulation of cold fluid adjacent to the downgoing slab. The extra cold fluid is apparent in a cross-section of temperature taken through the base of the 'weak

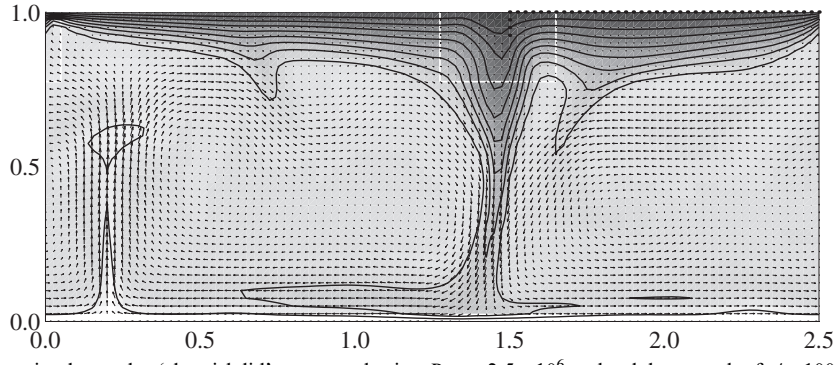

Figure 5. Snapshot of convection beneath a 'sluggish lid', generated using $Ra_m = 2.5 \times 10^6$ and a slab strength of $\eta_l' = 1000$. As in Fig. 3, greyscale and contours indicate temperature and the arrows indicate flow velocities. In this case, the resistance to bending slows the plate, which causes it to thicken and slow further because resistance to bending is greater for thicker plates. This runaway process decelerates the plate to $v_p' = 113$ and produces a bending dissipation of 27 per cent. The subsurface flow velocities, however, are significantly greater and indicate that convection is occurring beneath a 'sluggish lid'.

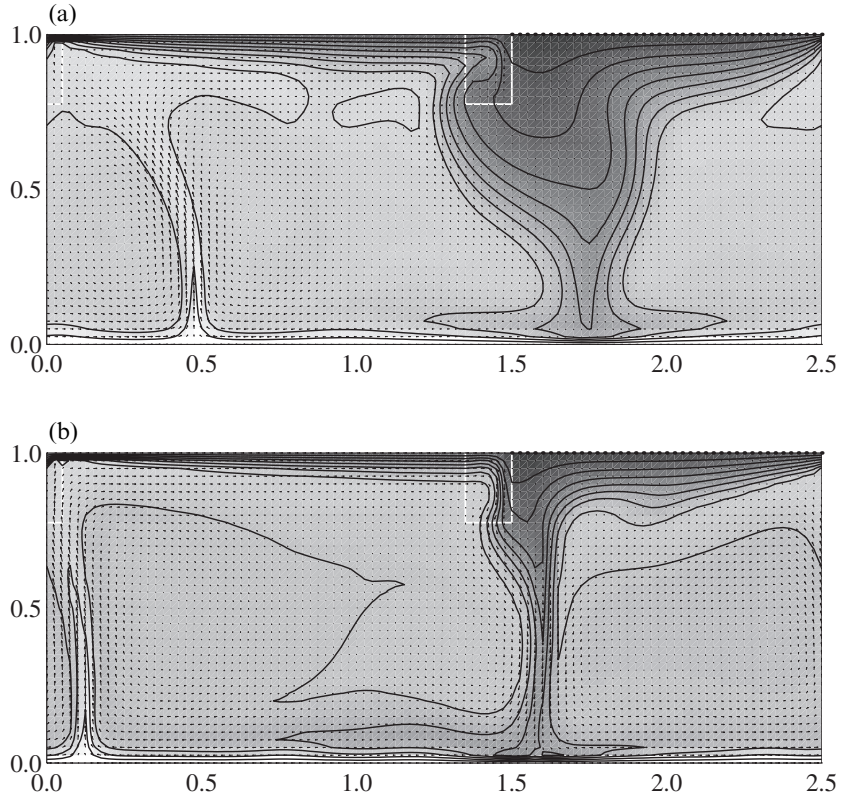

Figure 6. Similar to Fig. 3, but for a 'weak zone' representation of subduction. To implement the weak zone, the velocity boundary conditions used previously are removed and a temperature-independent viscosity of $\eta'_{wz}=1$ is imposed within a region six elements wide and nine deep between the oceanic and continental plates. Shown in (a) is the steady-state flow that results if the temperature dependence of viscosity is governed by an activation energy of $E_a=100$ kJ mol^{-1}. In this case, a large mass of cold material accumulates next to the weak zone, but the surface flow is still plate-like, giving a plate velocity of $v'_p=304$. Shown in (b) is the flow produced using $E_a=50$ kJ mol^{-1}. In this case, the plate velocity increases to $v'_p=922$ and the mass of cold material is smaller, but still present.

zone' (Fig. 7), which shows significantly thicker and colder material associated with a 'weak zone' (dotted line) than with a slab formed assuming either a strong ($\eta'_l=500$, dash-dotted line) or a weak ($\eta'_l=10$, dashed line) bending slab. The accumulation of cold material between the downgoing slab and the overriding plate is not consistent with the high heat flow and the volcanic activity observed at the surface, but the slab-induced mantle flow shown in Fig. 3 is (e.g. Davies & Stevenson 1992; McKenzie 1969).

We can also compare the temperature profiles of the slabs produced here to the profiles expected for the Earth (Fig. 7). To do this, we measure temperature as a function of horizontal distance using the temperature contours of Ponko & Peacock's (1995) detailed models of a slab's thermal structure. We make this measurement at a depth of 200 km because this depth is about twice that of the base of the oceanic plate, and is thus analogous to the depth of the previously plotted profiles in Fig. 7. To compare temperature profiles, we scale horizontal distance by the approximate thickness of the oceanic plate, which is about 100 km for Ponko & Peacock's (1995) results and about 0.1 in Fig. 3. We also scale the 1300 and 1400 °C temperature variations in Ponko & Peacock's (1995) models to the corresponding temperature variation of $T'=0.7$ in our models. The resulting temperature profiles (Fig. 7, solid lines) match the profiles for both the weak and the strong bending slabs better than they match the profile for the 'weak zone' subduction model. Furthermore, these slabs are produced using a larger and more reasonable activation energy of $E_a=100$ kJ mol^{-1}, while the 'weak zone' downwelling is produced using $E_a=50$ kJ mol^{-1}.

APPLICATION TO BOUNDARY LAYER THEORY

Boundary layer theory, as it is typically applied to the mantle, suggests that increases in the viscosity of the interior should result in slower plate velocities at the surface. We have shown, however, in a few example calculations, that plate velocity may also depend strongly on the dissipation associated with lithospheric bending as a plate subducts. We now investigate how changing the interior viscosity affects plate velocities for a convecting mantle in which bending of the lithosphere is an important source of dissipation. This analysis can be applied to a cooling Earth, which should experience an increase in its interior viscosity over time.

To vary the mantle Rayleigh number, we apply interior viscosities of $\eta'_{int}(T'_{int})=1/3$, 1 and 3. If the average interior mantle temperature were to remain constant at $T'=0.65$, these choices of viscosity would produce mantle Rayleigh numbers of $Ra_m=10^5$, 1×10^6 and 3.3×10^6. Typically, some warming causes Ra_m to increase slightly. Using the same starting temperature

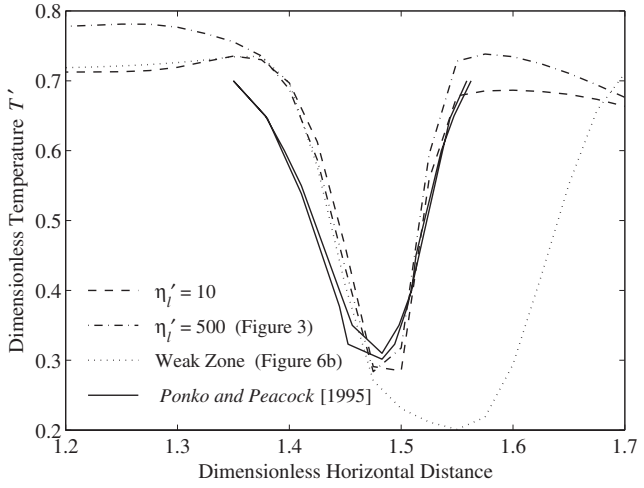

Figure 7. Temperature profiles through the slab for different implementations of subduction, measured in each case at the depth of the base of the subduction zone region (nine elements deep). The temperature profile is similar for the weak ($\eta_l'=10$, dashed line) and the strong (Fig. 3, $\eta_l'=500$, dash-dotted line) bending slabs, which are implemented using an activation energy of $E_a=100$ kJ mol^{-1}. The profile for the 'weak zone' implementation that uses a smaller activation energy of $E_a=50$ kJ mol^{-1} (Fig. 6b, dotted line) is significantly thicker because of the mass of cold fluid that accumulates next to the weak zone. For comparison, we show temperature profiles measured from Ponko & Peacock's (1995) two thermal models of the slab beneath Alaska (solid lines), which have been rescaled as described in the text to allow a comparison to our results.

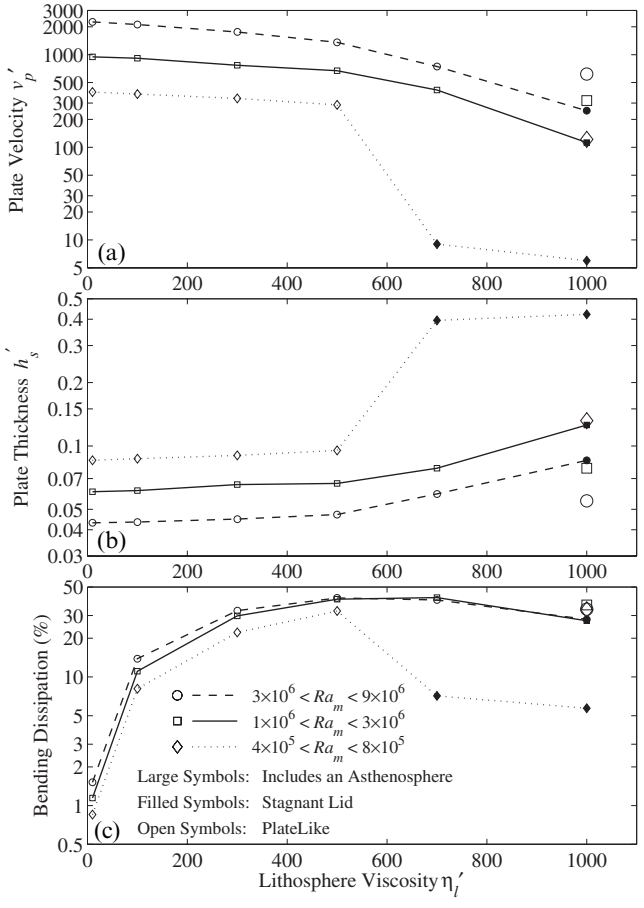

Figure 8. The variation of (a) plate velocity v_p', (b) plate thickness h_s' and (c) the fraction of the total energy dissipation that occurs as plate bending as a function of the effective viscosity of the bending plate η_l'. All results are shown on a semi-log plot and the three different lines indicate the grouping of results by mantle Rayleigh number Ra_m. Filled symbols indicate calculations that produce convection beneath a 'sluggish lid' while open symbols indicate plate-like behaviour. The large symbols denote runs in which a low-viscosity asthenosphere is included, which has the effect of limiting plate thickness and thus preventing the formation of a 'sluggish lid'. Temperature and flow fields for the three plate-like calculations with an asthenosphere are shown in Figs 9 and 10.

field as before, we initiate convection using different lithospheric viscosities η_l' and allow convection to occur until a steady state is reached. At steady state and for each lithosphere viscosity, we measure the average plate velocity v_p', the plate thickness h_s' and the fraction of dissipation occurring as bending (Fig. 8).

Several trends are noteworthy. First, as predicted by boundary layer theory, plate velocity increases with increasing Ra_m (Fig. 8a), which leads to a thinner oceanic plate (Fig. 8b). As we found above for a single value of Ra_m, a significant decrease in v_p' (by nearly a factor of two) is observed as the lithosphere viscosity increases from $\eta_l'=10$ to $\eta_l'=500$ (Fig. 8a). This decrease in plate velocity is accompanied by an increase in plate thickness h_s' (Fig. 8b) and by an increase in the fraction of the total dissipation that occurs as bending (Fig. 8c). Once lithosphere viscosity increases beyond $\eta_l'=500$, plate velocities decrease and plate thicknesses increase more rapidly with increasing lithosphere viscosity (Fig. 8a). This change is characteristic of 'sluggish lid' convection (shown as solid symbols in Fig. 8) and is accompanied by thicker plates (Fig. 8b) and decreased bending dissipation (Fig. 8c).

We can compare the trends observed in Fig. 8 with those predicted by Conrad & Hager (1999b), who discussed a variation of standard boundary layer theory that includes viscous bending of the lithosphere at a subduction zone. By balancing Φ^{pe} with Φ_m^{vd} and Φ^{vd_l}, plate velocity, v_p, can be expressed as

$$v_p=\frac{\rho g\alpha(T_{int}-T_s)l_s h_s/\sqrt{\pi}}{C_m\eta_m+2\eta_l(h_s/R)^3}\,. \tag{17}$$

The thickness of a plate at the time of subduction is determined by half-space cooling, which leads to a relationship between plate thickness and plate velocity of

$$h_s=2\sqrt{\kappa L/v_p}\qquad\text{or}\qquad v_p=\frac{4\kappa L}{h_s^2}\,. \tag{18}$$

Combining eqs (17) and (18) yields an expression for the plate thickness, h_s:

$$h_s=\left(\frac{1}{Ra_m}D^3\,\frac{4\sqrt{\pi}C_m Ra_l L/D}{Ra_l-8\sqrt{\pi}L/l_s}\right)^{(1/3)}\,, \tag{19}$$

where, following Conrad & Hager (1999b), Ra_l is a 'lithospheric' Rayleigh number,

$$Ra_l=\frac{\rho g\alpha(T_{int}-T_s)R^3}{\eta_l\kappa}\,. \tag{20}$$

Using eqs (18) and (19), we can write the relationship between mantle Rayleigh number and both plate thickness and plate

velocity in terms of a power-law,

$$h_s \sim Ra_m^{-\beta} D \qquad \text{and} \qquad v_p \sim Ra_m^{2\beta} \kappa / D\,, \tag{21}$$

where β is a power-law exponent, given in this case by $\beta = 1/3$. This value for β was originally obtained from boundary layer theory that did not include bending slabs (e.g. Turcotte & Oxburgh 1967), but the above analysis shows that this value should apply even if the bending dissipation is significant. If, however,

$$Ra_l \leq 8\sqrt{\pi} L / l_s\,, \tag{22}$$

it is the clear from eq. (19) that the plate thickness, h_s, becomes infinite, in which case the plate velocity, v_p, approaches zero, and a sluggish lid is formed. This condition occurs when the bending dissipation is sufficiently large that v_p as expressed by eq. (17) is always smaller than v_p as expressed by eq. (18) (e.g. Conrad & Hager 1999a). By applying eq. (20) to eq. (22) and making the lithosphere viscosity dimensionless according to eq. (9), we can rewrite the condition for a sluggish lid as

$$\eta_l' \geq 10^6 \frac{R^3}{D^3} \frac{l_s}{8\sqrt{\pi} L}\,. \tag{23}$$

To apply this equation to our model, we set $l_s = D$, $L/D = 1.5$ and $R/D = 0.225$. This yields a condition for a sluggish lid of $\eta_l' \geq 540$, which is independent of mantle viscosity. We observe a transition to a sluggish lid in the range $500 < \eta_l' < 700$ for the smallest range of Ra_m in Fig. 8, which agrees with theory. For higher Ra_m, the transition occurs at slightly larger η_l', indicating some dependence on Ra_m. This deviation from theory may be due to thinning of the oceanic lithosphere by convective erosion at its base, as discussed below.

For lithosphere viscosities smaller than those for which a sluggish lid develops, the fraction of total energy dissipation that occurs as bending is independent of mantle Rayleigh number (Fig. 8c). This observation can be predicted by first writing an expression for the fraction of dissipation that bending represents, and rewriting this expression in terms of Ra_l:

$$\frac{\Phi_l^{vd}}{\Phi_m^{vd} + \Phi_l^{vd}} = \frac{2\eta_l h_s^3 / R^3}{C_m \eta_m + 2\eta_l h_s^3 / R^3} = \frac{2h_s^3}{C_m D^3 Ra_l / Ra_m + 2h_s^3}\,. \tag{24}$$

Applying eq. (19) to eq. (24) yields

$$\frac{\Phi^{vd}}{\Phi_m^{vd} + \Phi_l^{vd}} = \frac{8\sqrt{\pi} L / D}{Ra_l}\,. \tag{25}$$

Thus, the fraction of the total dissipation that bending represents should not depend on Ra_m, but instead on the properties of the lithosphere expressed by Ra_l. This is indeed what we observe; this quantity depends more on η_l' than on Ra_m in Fig. 8(c). For lithospheric bending that approaches the 'sluggish lid' limit, as defined by eq. (22), plates are infinitely thick, so the bending dissipation is 100 per cent. For flow with mobile plates of finite thickness, the maximum bending dissipation should be smaller than this. Here we observe a maximum value of about 40 per cent (Fig. 8c), which is smaller than the 50–60 per cent value that Conrad & Hager (1999a) estimated for the mantle based on the Earth's distribution of surface plate velocities. Their estimate, however, ignores flow beneath continents, which should also be driven by subducting slabs. To include this portion of the flow, the deep mantle portion of Conrad & Hager's (1999a) energy budget analysis should be increased by about two-thirds, which corresponds to the approximate ratio of continent area to ocean area for the Earth, and also for this analysis. Doing this decreases their estimate of the fraction of bending dissipation to 35–45 per cent, which is consistent with the measurements made here.

THE ROLE OF AN ASTHENOSPHERE

The resistance to plate bending leads to sluggish lid convection because it slows plate motions, thickening plates and increasing the bending resistance further. This runaway process thus requires the bending resistance to increase as plate motions are slowed, a consequence that can be interrupted in one of two ways. First, various stress-weakening constitutive relations may cause the slab's effective viscosity to decrease once bending stresses increase beyond a certain point. Karato *et al.* (2000) suggested that such weakening may place a maximum on the total amount of viscous dissipation that can occur within the bending slab. Once this maximum value is reached, increases in slab age, and thus thickness, do not change the bending resistance, which breaks up the feedback mechanism that leads to a sluggish lid. Another mechanism, proposed by Conrad & Hager (1999a,b), could be a process that limits the oceanic plate thickness to some maximum value. In this case, once the oceanic plate thickness saturates, the plate bending resistance would remain constant even for a slab with a Newtonian viscosity.

There is evidence, in fact, that the thickness of oceanic plates is limited by some process. For example, it has been proposed that plates reach a maximum thickness after about 80 myr, the age at which the linear relationship between seafloor depth and the square root of its age is observed to break down (e.g. Parsons & Sclater 1977; Stein & Stein 1992). One mechanism that might limit plate thicknesses is convective erosion at the base of the oceanic lithosphere (e.g. Davaille & Jaupart 1994; Marquart *et al.* 1999; Parsons & McKenzie 1978), which, if important, would remove cold material below about 100 km, the thickness given by eq. (15) for a plate 80 Myr old. Convective instability beneath the oceanic lithosphere could be facilitated by the presence of a low-viscosity asthenospheric channel that may exist between 100 and 400 km depth (e.g. Hager 1991). Although some controversy is associated with the seafloor flattening observation and the process by which it occurs (e.g. Stein & Stein 1997), we investigate the effects of limiting the maximum plate thickness by adding a low-viscosity asthenosphere to our calculations.

We introduce an asthenosphere by imposing temperature-dependent viscosity with a value a factor of 10 smaller than that of the rest of the mantle for the fourth–ninth elements from the surface between the ridge and the subduction zone (Fig. 1). Because of its temperature-dependent viscosity, the mantle above this low-viscosity asthenosphere continues to behave as a rigid plate. We employ an effective viscosity for bending of $\eta_l' = 1000$, which produces a 'sluggish lid' in calculations without an asthenosphere (Fig. 8), and vary the mantle viscosity as before. The results (Fig. 8, large symbols) show plate thicknesses that are smaller than are observed for the sluggish lid cases (Fig. 8b) and greater plate velocities (Fig. 8a). Thus, the presence of an asthenosphere facilitates plate-like motion in calculations that would otherwise produce sluggish lid convection.

The velocity and temperature fields produced by these calculations (Figs 9 and 10) demonstrate how the asthenospheric channel prevents sluggish lid formation. Because the viscosity of the asthenosphere region is smaller than that of the oceanic plate above it, any cold fluid in the asthenosphere is gravitationally more unstable than it is in the overlying plate, and thus can be removed more easily by small-scale convection. The downwellings beneath the oceanic plate in Figs 9 and 10 demonstrate this process of convective removal of cold fluid from the asthenosphere. Because plates cannot grow thick, slow plates do not become yet slower because of an additional resistance to bending, and a sluggish lid is avoided. However, because the plate viscosity is high, making the bending resistance large, the plates in these calculations move slowly, which permits flow velocities in the interior fluid to be greater than those of the surface plate (Figs 9 and 10), a pattern found for sluggish lid convection (Fig. 5). A detailed look at the subduction zone region (Fig. 10b), however, shows that surface flow is indeed plate-like. The deformation of the slab as it descends is a property of the dependence of slab strength on temperature, a slab characteristic that is not well understood and cannot be modelled accurately here. A slightly different viscosity law might produce slabs that are strong enough to remain largely intact at high Rayleigh number, despite being attached to slow-moving surface plates.

If small-scale convection or some other process limits the thickness of plates to some maximum value h_m, the power-law relationships given in eq. (21) should apply, but with a value of $\beta < 1/3$. To show this, we note that if $h_s = h_m$, the plate velocity given by eqs (17) and (18) is no longer relevant. The relative importance of the two terms in the denominator of eq. (17) depend on the fraction of dissipation occurring as bending. This can be estimated from eq. (24), which, if Ra_m is sufficiently large, shows that the bending resistance should be dominant, even for plate-like flow. In this case, as discussed by Conrad & Hager (1999b), the plate velocity, as given by eq. (17), depends only on the effective viscosity of the lithosphere and the buoyancy of the slab, and is thus independent of mantle viscosity and Rayleigh number. As a result, we expect β in eq. (21) to be zero.

We test this prediction by measuring the average plate velocity and plate thickness as a function of Rayleigh number (Fig. 11) for both weak ($\eta_l' = 10$) and strong ($\eta_l' = 500$) bending plates, and for a strong bending plate with an asthenosphere ($\eta_l' = 1000$). Some uncertainty is associated with these measurements because, as shown in Fig. 4, both v_p and h_s vary significantly with time, making the measurement of a 'typical' value somewhat problematic. As before, we measure an average value at steady state, but include error bars with a length of one standard deviation to show an the approximate range of uncertainty. As predicted, the calculations without an asthenosphere ($\eta_l' = 10$ and 500) produce values of β near 1/3, even for a strong bending plate. Some variation is observed, but the expected slopes associated with $\beta = 1/3$ could easily fit within the error estimates. The calculation with an asthenosphere, however, shows smaller estimates for β of about 0.185 for

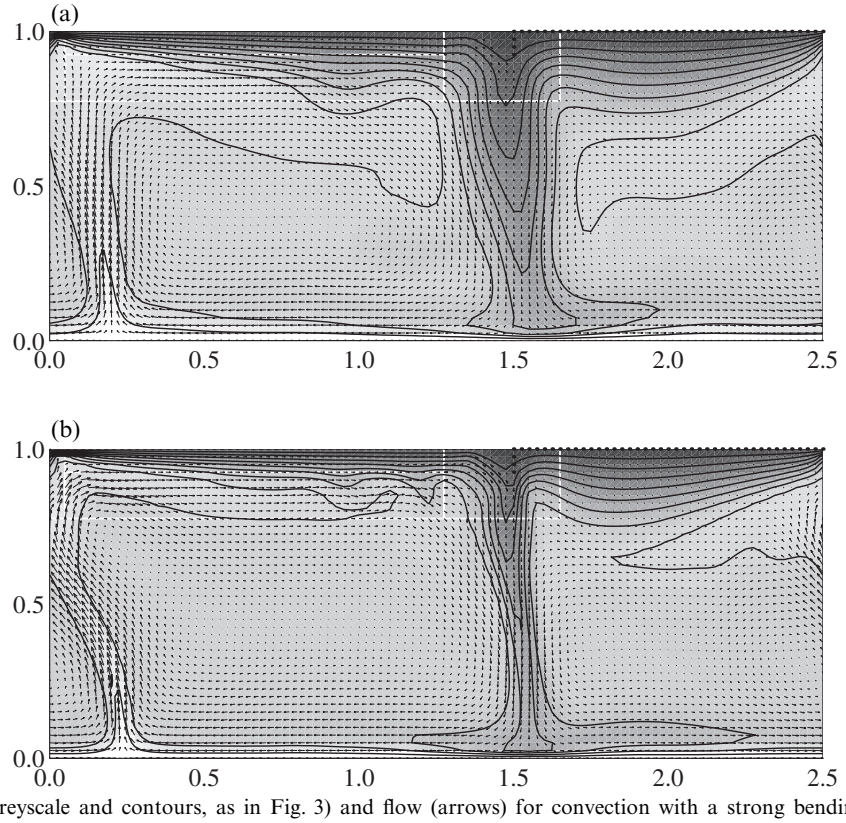

Figure 9. Temperature (greyscale and contours, as in Fig. 3) and flow (arrows) for convection with a strong bending plate ($\eta_l' = 1000$) and an asthenosphere with temperature-dependent viscosity that is factor of 10 smaller than that of the mantle for a given temperature. Shown are results for (a) a mantle Rayleigh number of $Ra_m = 6.3 \times 10^5$ (large open diamond in Fig. 8) and (b) a mantle Rayleigh number of $Ra_m = 1.9 \times 10^6$ (large open square in Fig. 8). In both cases, small-scale instability occurs beneath the oceanic plate once it begins to thicken into the lower-viscosity asthenosphere. This process removes cold fluid from the base of the plate and limits the thickness to which a plate can grow. Because thick plates cannot form, 'sluggish lid' convection is averted.

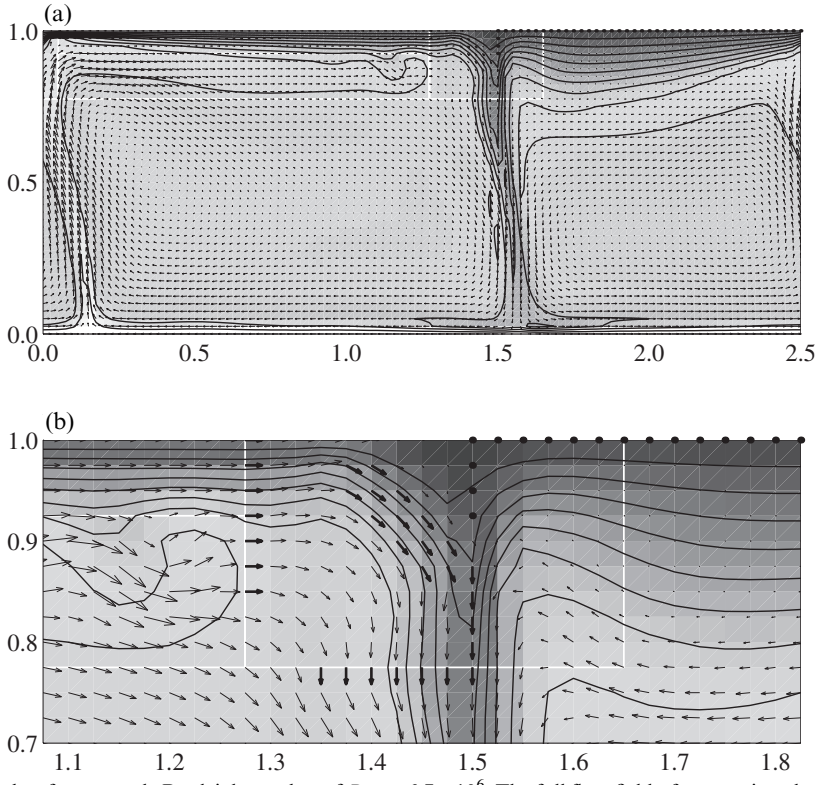

Figure 10. Similar to Fig. 9, but for a mantle Rayleigh number of $Ra_m = 6.7 \times 10^6$. The full flow field of convection shown in (a) features some of the attributes of the 'sluggish lid' convection shown in Fig. 5 because the flow velocities in the mantle interior are larger than those associated with the plate. The detailed view of the subduction zone region in (b), however, shows that surface motion is, in fact, plate-like. As we found for smaller Rayleigh number in Fig. 9, small-scale instability removes the basal portions of the oceanic plate and prevents the development of a full-scale sluggish lid.

velocity and 0.22 for plate thickness. In both cases, calculating a slope using only data from the two larger values of Ra_m would produce an even smaller measurement of β (Fig. 11). Thus, the addition of an asthenosphere serves to make plate velocity and thickness less dependent on mantle Rayleigh number. Theory predicts a value of $\beta = 0$ if plate thickness is constant. We can see that our implementation of an asthenosphere does not produce constant plate thickness with varying Rayleigh number (Fig. 11b), which explains measured values of $\beta > 0$ for velocity (Fig. 11a).

HEAT FLOW AND THE THERMAL EVOLUTION OF THE EARTH

The relationship between plate velocities and mantle Rayleigh number has implications for the Earth's thermal evolution because this relationship influences the efficiency of convective heat transport. The Earth's primary mechanism for heat loss is the cooling of oceanic plates, for which the total heat flow can be written as

$$N = 2D\left(\frac{v_p}{\pi\kappa L}\right)^{(1/2)} \sim Ra_m^{\beta}, \tag{26}$$

which uses the relationship between v_p and Ra_m given by eq. (21) (e.g. Turcotte & Schubert 1982, pp. 280–283). Here the heat flow is given by N and is made dimensionless by dividing by the heat flow expected from conduction occurring alone. Thus, N is analogous to a Nusselt number, which measures the efficiency of heat transfer by convection. The response of mantle heat flow to changes in Ra_m is measured by the power-law exponent β, which, as discussed above, should have a value of $\beta \sim 1/3$ if boundary layer theory applies. Thus, as the Earth cools, Ra_m should decrease because the interior mantle viscosity depends on temperature. If $\beta > 0$, this change should be accompanied by a decrease in N, which slows the mantle's rate of cooling. This negative feedback mechanism has the effect of preventing rapid changes in the temperature of the interior. If β is smaller than the value of 1/3 predicted by boundary layer theory, this temperature-regulating mechanism is diminished, and more rapid changes in mantle temperature are permitted. Thus, the response of convection to changes in mantle interior viscosity, measured by β, determines the course of Earth's thermal evolution.

The variation of either plate velocity or plate thickness with mantle Rayleigh number (Fig. 11) produces $\beta \sim 1/3$ for a mantle with no asthenosphere and subduction zones that are either weak ($\eta_l' = 10$) or strong ($\eta_l' = 500$), but $\beta < 1/3$ for calculations that include an asthenosphere. The value of β applicable for convective heat transfer, and thus for Earth's thermal evolution, can also be estimated directly by measuring the heat flow out of the surface of the finite element calculation. We make this measurement, using the technique developed by Ho-Liu *et al.* (1987), for both the entire grid surface (Fig. 12a) and the oceanic plate alone (Fig. 12b). In both cases, we observe a smaller value of β for calculations that include an asthenosphere. All of the measurements are smaller than the

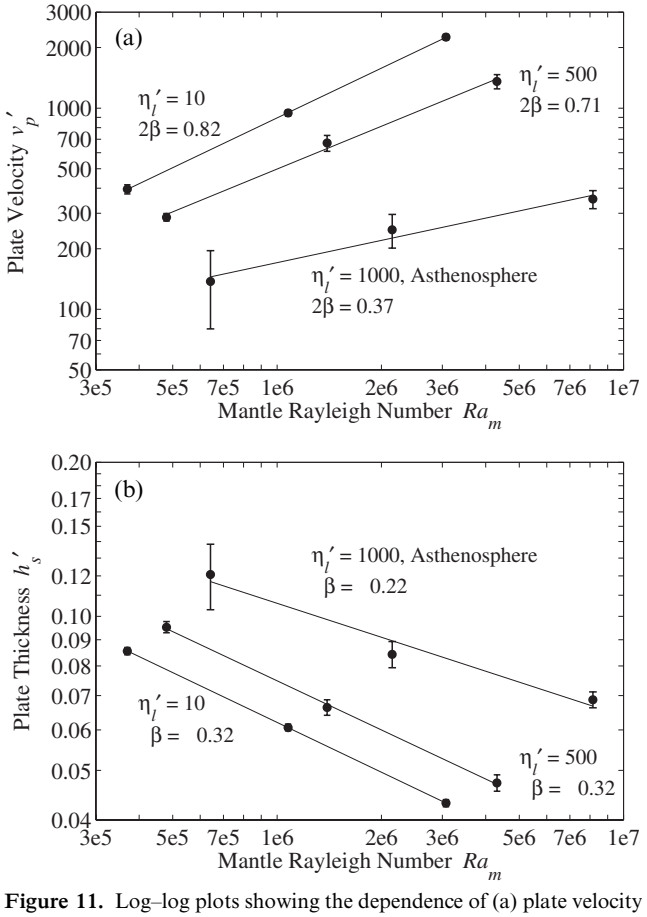

Figure 11. Log–log plots showing the dependence of (a) plate velocity v_p' and (b) plate thickness h_s' on mantle Rayleigh number Ra_m. Shown are selected results from Fig. 8, for a weak bending slab ($\eta_l' = 10$), a strong bending slab ($\eta_l' = 500$) and a strong bending slab ($\eta_l' = 1000$) for a calculation that includes an asthenosphere. As shown in Fig. 4, both v_p' and h_s' vary significantly with time. Thus, we plot their mean values for the time period after which steady state has been achieved. Error bars show one standard deviation from this mean, and thus give an estimate of the uncertainty associated with each measurement. Lines through the points are the least-squares linear fits to the three data points. According to eq. (21), v_p' should depend on $Ra_m^{2\beta}$ and h_s' should depend on $Ra_m^{-\beta}$. Thus, we express the best-fit slope of each line in terms of the power-law exponent β, which, if boundary layer theory applies, should have a value of $\beta = 1/3$. The measurements made here indicate that in general $\beta \sim 1/3$, even if the bending resistance is large ($\eta_l' = 500$) but $\beta < 1/3$ for the calculations that include an asthenosphere.

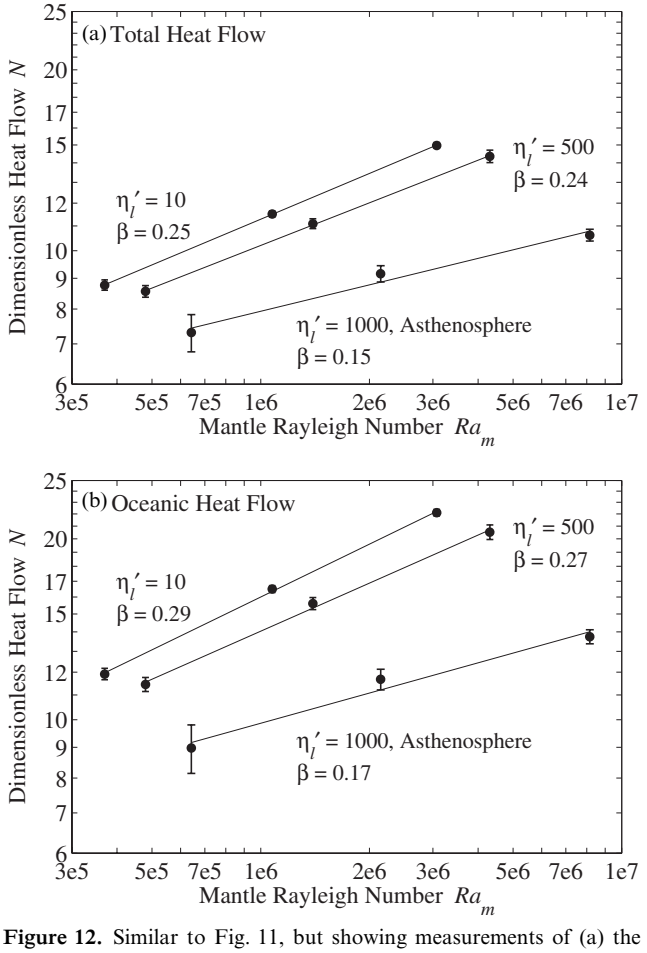

Figure 12. Similar to Fig. 11, but showing measurements of (a) the total heat flow and (b) the heat flow out of the oceanic plate as a function of mantle Rayleigh number Ra_m. Here heat flow is expressed as the dimensionless quantity N, which is normalized by the solution for conduction alone and is thus analogous to a Nusselt number. The slope, β, is measured as shown in Fig. 11, and boundary layer theory predicts $\beta = 1/3$. This slope is smaller than the prediction of boundary layer theory in all cases, but particularly so for the calculations that include an asthenosphere.

expected value of $\beta \sim 1/3$, presumably because of heat transfer mechanisms that are not associated with the formation of the oceanic plate. Such mechanisms certainly apply for the total heat flow measurement (Fig. 12a) because a significant fraction of this heat flow occurs as conduction through the continent. This portion of the total heat flow should depend weakly on Ra_m, which explains the smaller measured values of β for the total heat flow (compare Figs 12a and b). Conduction through (as opposed to cooling of) the oceanic plate may occur as well, which could explain the measurements of $\beta < 1/3$ there (Fig. 12b). Most of the oceanic heat flow, however, occurs close to the ridge where the plate is thin and cooling of the oceanic plate dominates. This portion of the heat flow is related to $v_p^{1/2}$, as in eq. (26). For the calculation that includes an asthenosphere, we observe a diminished dependence of v_p' on Ra_m (Fig. 11a) because the plate velocity is determined by η_l' rather than by η_m'. The measurement of $\beta \sim 0.17$ using oceanic heat flow (Fig. 12b) can be attributed to the same effect.

For a cooling Earth, lithosphere viscosity should depend on surface temperatures, which are thought to have deviated by less than 50 °C since the Archaean (e.g. Holland & Kasting 1992). This implies constant lithosphere viscosity, so if convection rates depend on this viscosity, plate velocities, and thus mantle heat flow, should be more constant as the Earth cools than they would be if plate velocities depended solely on the mantle viscosity. Thus, the calculations for which $\beta < 1/3$ predict less variation in heat flow over time. Small β is not, however, produced by a large bending resistance alone. Instead, the bending resistance must remain constant despite changes in Ra_m, which requires some mechanism for maintaining either constant subducting plate thickness or diminished effective viscosity for thicker plates. As discussed above, either of these two mechanisms is a viable possibility for the Earth.

A diminished value of β has been proposed as a mechanism for explaining an apparent discrepancy between estimates of

Earth's current rate of secular cooling and models of the Earth's thermal history that are based on parametrized convective heat transport (e.g. Christensen 1984, 1985; Conrad & Hager 1999b). The former is typically expressed by the Urey number, which is the ratio of the mantle's current rate of heat production to its total surface heat flow. This ratio has been estimated to have a present-day value of about 0.5 based on estimates of the concentration of internal heat sources for a primitive mantle (e.g. Christensen 1985). However, if $\beta = 1/3$, the mantle is efficient at regulating its internal temperature, which implies a small amount of present-day secular cooling. In fact, thermal history calculations suggest that if more than about 15 per cent of the total mantle heat flow represents secular cooling (Urey number of 0.85), a value of $\beta = 1/3$ produces a thermal catastrophe only 1 or 2 billion years ago (e.g. Christensen 1985). If, however, $\beta < 1/3$, the mantle is less efficient at regulating its temperature and thus can cool more rapidly, permitting smaller Urey ratios. Christensen (1985) estimates that Urey ratios of ~ 0.5 are acceptable if $\beta \sim 0.1$. This is smaller than the estimates of β made here, but it is possible that, as predicted theoretically by Conrad & Hager (1999b), Earth-like combinations of mantle Rayleigh number, lithosphere strength and maximum plate thickness could yield smaller β. Such calculations, however, require computational power beyond the scope of this study.

Christensen (1984, 1985) also observed $\beta < 1/3$ in convection calculations that included temperature-dependent viscosity. These calculations, however, paid no special attention to subduction zones, and thus are better described by 'sluggish lid' convection without realistic slabs or surface plates. Our model in which plate motions are resisted by lithospheric bending at subduction zones produces Earth-like plate and slab behaviour, but still produces decreased β. Other models that generate reasonable subduction by imposing 'weak zones' (e.g. Gurnis 1989) do not yield small β because plate velocities depend on mantle viscosity.

DISCUSSION

The method for implementing subduction developed here incorporates an assumed model for subduction zone deformation into a small region of a finite element grid. Thus, it provides a useful method for incorporating Conrad & Hager's (1999b) study of viscous bending for a subducting plate into a larger-scale convecting system without requiring additional numerical resolution. Because this method parametrizes subduction zone deformation using an energy balance, other models for this deformation can also be easily implemented, as long as an expression for the energy they dissipate can be written in terms of the gross physical properties of the subduction zone such as the thickness, velocity and temperature structure of the subducting plate. In particular, it would be useful to study the effects of different rheologies that include stress weakening or a maximum yield stress.

We enforce a realistic geometry for subduction by imposing velocity boundary conditions in the vicinity of the subduction zone. As we have shown, this approach produces a more realistic thermal field for the subducted slab than is produced by other methods that employ pure shear at the surface. Using velocity boundary conditions, however, has the disadvantage that the dip angle must be pre-imposed and constant with time. We have found that by using different sets of velocity boundary conditions, subduction with a dip angle smaller than the 90° angle used here can be implemented fairly easily. If an expression for the proper dip angle could be determined from the characteristics of mantle flow, a more fully dynamic representation of subduction could be implemented by imposing the proper set of velocity boundary conditions at each time step.

Our method for implementing subduction uses an energy balance between viscous dissipation and potential energy release to determine the rate of subduction. Because this energy balance is determined globally, it is unclear how to implement multiple subduction zones. For example, in a model with two subduction zones, some method of dividing the viscous dissipation and potential energy release must be developed so that an expression for the appropriate subduction rate can be determined for both subduction zones. If the flow associated with each subduction zone were independent, then a valid solution could be determined by imposing zero velocity at one subduction zone and using the energy balance method globally to determine the velocity for the other. The velocity for the first subduction zone could be determined by the same method, and then the two velocities could be imposed simultaneously to advance the flow. We would expect an interaction, however, between the flow associated with neighbouring subduction zones, so this method might miss some important aspects of convection in a multiple subduction zone system.

Due to computational constraints, we were unable to study Earth-like Rayleigh numbers of 10^7–10^8. Nevertheless, we can apply our analysis to the Earth in several ways. For example, we have found, and theory predicts, that the maximum amount of bending dissipation that can occur before the formation of a sluggish lid, measured here at ~ 40 per cent, should be nearly independent of mantle Rayleigh number. We have also shown that if some mechanism limits the total bending resistance, sluggish lid convection is replaced by convection with mobile surface plates whose velocity is determined by lithospheric strength. Thus, if such a mechanism is present, the condition for the onset of sluggish lid convection also indicates the onset of convection characterized by plate velocities that are independent of mantle Rayleigh number. This condition, predicted by Conrad & Hager (1999b) and verified numerically here, is given by eq. (22) as $Ra_l < 8\sqrt{(\pi)}L/l_s$, a condition that does not depend on mantle interior viscosity. For the Earth, we estimate $\rho = 3300$ kg m^{-3}, $g = 10$ m s^{-2}, $\alpha = 3 \times 10^{-5}$ K^{-1}, $T_{\rm int} - T_s = 1300$ K, $\kappa = 10^{-6}$ m^2 s^{-1}, $D = 2500$ km, $R = 200$ km (Bevis 1986, 1988; Isacks & Barazangi 1977), $l_s = 1000$ km and $L = 5000$ km. Applying these values to eqs (20) and (22), we estimate a critical value for the effective lithosphere viscosity of $\eta_l \sim 10^{23}$ Pa s. This estimate is consistent with other estimates of η_l by De Bremaecker (1977) and Conrad & Hager (1999a) and is a value typically used in studies that generate subduction by introducing faults to strong oceanic lithosphere (e.g. Zhong & Gurnis 1995a,b; Zhong *et al.* 1998). Because the mantle's viscosity is temperature-dependent, we expect η_l to be somewhat greater than the average viscosity of the underlying mantle. Estimates of the latter are of the order of 10^{21} Pa s, so an effective viscosity for bending of $\sim 10^{23}$ Pa s is perhaps not unreasonable.

Convection at high Rayleigh numbers may also have characteristics that cannot be adequately modelled here. In our models, we could implement higher Rayleigh numbers by decreasing the mantle viscosity. This would induce additional small-scale convection beneath the oceanic lithosphere, even if

we did not impose an asthenosphere. Thus, for the Earth, a low-viscosity asthenosphere might not be needed for oceanic plate thicknesses to be limited by convective erosion at their base. On the other hand, decreasing the mantle viscosity in our models would also serve to weaken the downgoing slab. In our lowest-viscosity calculations that include an asthenosphere (Fig. 10), we found that the slab weakens considerably as it descends, causing it to pull away from the subduction zone. This behaviour resembles that of a 'sluggish lid', and decreasing the mantle viscosity further might cause the slab to fall away from the subduction zone altogether. Certainly both small-scale convection and the deformation of a downgoing slab are complicated processes that, like plate bending in subduction zones, depend on the details of the rheology that affect them. We expect that neither is adequately modelled in these calculations but that both should be essential aspects of the style of convection studied here.

CONCLUSIONS

The method developed here for implementing subduction in a numerical model of convection parametrizes the deformation of a subduction zone within a small region of a finite element grid. Because we do not attempt to model this deformation accurately, but instead rely on more detailed local models to do this, we can easily investigate the effects of different types of subduction zone deformation on mantle flow. To demonstrate the importance of subduction zones to convection, we implement a model for bending a viscous plate within the subduction zone. In particular, we study convection in which oceanic plates maintain their strength as they deform within the subduction zone. This type of 'strong' subduction zone cannot be investigated using standard methods for implementing subduction because these methods typically require convergent plate boundaries to be weak.

Using this method, we have shown that plate-like surface motions are produced even if the bending deformation associated with subduction dissipates $\sim$40 per cent of the mantle's total convective energy, in which case plate velocities are slowed significantly. If the bending dissipation increases beyond this level, plates are slowed further and become so old and thick at the time of subduction that the bending resistance prevents plates from actively participating in convection, causing flow to occur beneath a 'sluggish lid'. If, however, some process prevents the bending resistance from increasing with plate age, plate-like convection can be maintained. One such process could be small-scale convection beneath old oceanic lithosphere, which could limit the thickness to which plates can grow, and thus prevent old plates from becoming too thick to subduct. Various stress-weakening rheologies may also be able to weaken the subducting slab if it begins to become too thick. Whatever process is involved, it could be an essential aspect of mantle convection that facilitates plate tectonic motions at the Earth's surface, and thus enables Earth to avoid the 'sluggish lid' or 'stagnant lid' convection that might apply for Venus or Mars.

If the bending resistance saturates at some constant maximum value, the effective lithosphere viscosity that applies for plate bending should largely determine the velocity of plates. We have shown that, for the Earth, an effective lithosphere viscosity of 10^{23} Pa s should be sufficient to control plate velocities. If this viscosity remains constant despite the increases in mantle interior viscosity that we expect for a cooling Earth, plate velocities, and thus mantle heat flow, should change little over time. Because convection rates are not determined by the mantle interior viscosity, the temperature-regulating feedback mechanism that slows convective heat transfer as the Earth cools is diminished. Thus, an Earth with 'strong' subduction zones should experience more rapid changes in temperature, which is consistent with geochemical evidence that about half of present-day mantle heat flow represents secular cooling. As a result, we conclude that the deformation associated with plate bending at subduction zones could be an essential aspect of mantle convection, particularly if the lithosphere remains strong as it subducts. Not only might this additional bending resistance slow plate motions, but it could control the efficiency of convective heat transport, and thus determine the thermal evolution of the Earth.

ACKNOWLEDGMENTS

This work was supported in part by National Science Foundation grants 9506427-EAR and EAR-9905779, by a National Science Foundation Graduate Research Fellowship (CPC), and by the Los Alamos Institute of Geophysics and Planetary Physics (BHH). We thank Louis Moresi and an anonymous referee for constructive reviews and Peter Molnar for insightful comments that helped to improve the manuscript.

REFERENCES

Backus, G.E., 1975. Gross thermodynamics of heat engines in deep interior of Earth, *Proc. Nat. Acad. Sci. USA,* **72,** 1555–1558.

Becker, T.W., Faccenna, C., O'Connell, R.J. & Giardini, D., 1999. The development of slabs in the upper mantle: insights from numerical and laboratory experiments, *J. geophys. Res.,* **104,** 15 207–15 226.

Bercovici, D., 1996. Plate generation in a simple model of lithosphere-mantle flow with dynamic self-lubrication, *Earth planet. Sci. Lett.,* **144,** 41–51.

Bercovici, D., 1998. Generation of plate tectonics from lithosphere-mantle flow and void-volatile self-lubrication, *Earth planet. Sci. Lett.,* **154,** 139–151.

Bevis, M., 1986. The curvature of Wadati-Benioff zones and the torsional rigidity of subducting plates, *Nature,* **323,** 52–53.

Bevis, M., 1988. Seismic slip and down-dip strain rates in Wadati-Benioff zones, *Science,* **240,** 1317–1319.

Bunge, H.-P. & Richards, M.A., 1996. The origin of large scale structure in mantle convection: effects of plate motions and viscosity structure, *Geophys. Res. Lett.,* **23,** 2987–2990.

Chandrasekhar, S., 1961. *Hydrodynamic and Hydromagnetic Stability,* Oxford University Press, Oxford.

Chapple, W.M. & Forsyth, D.W., 1979. Earthquakes and bending of plates at trenches, *J. geophys. Res.,* **84,** 6729–6749.

Chapple, W.M. & Tullis, T.E., 1977. Evaluation of the forces that drive the plates, *J. geophys. Res.,* **82,** 1967–1984.

Christensen, U.R., 1984. Heat transport by variable viscosity convection and implications for the Earth's thermal evolution, *Phys. Earth planet. Inter.,* **35,** 264–282.

Christensen, U.R., 1985. Thermal evolution models for the Earth, *J. geophys. Res.,* **90,** 2995–3007.

Conrad, C.P. & Hager, B.H., 1999. Effects of plate bending and fault strength at subduction zones on plate dynamics, *J. geophys. Res.,* **104,** 17 551–17 571.

Conrad, C.P. & Hager, B.H., 1999. The thermal evolution of an Earth with strong subduction zones, *Geophys. Res. Lett.,* **26,** 3041–3044.

Davaille, A. & Jaupart, C., 1993. Transient high-Rayleigh-number thermal convection with large viscosity variations, *J. Fluid. Mech.,* **253,** 141–166.

Davaille, A. & Jaupart, C., 1994. Onset of thermal convection in fluids with temperature-dependent viscosity: application to the oceanic mantle, *J. geophys. Res.,* **94,** 19 853–19 866.

Davies, G.F., 1988. Role of the lithosphere in mantle convection, *J. geophys. Res.,* **93,** 10 451–10 466.

Davies, G.F., 1989. Mantle convection model with a dynamic plate: topography, heat flow and gravity anomalies, *Geophys. J. Int.,* **98,** 461–464.

Davies, J.H. & Stevenson, D.J., 1992. Physical model of source region of subduction zone volcanics, *J. geophys. Res.,* **97,** 2037–2070.

De Bremaecker, J.-C., 1977. Is the oceanic lithosphere elastic or viscous?, *J. geophys. Res.,* **82,** 2001–2004.

Engdahl, E.R. & Scholz, C.H., 1977. A double Benioff zone beneath the central Aleutians: an unbending of the lithosphere, *Geophys. Res. Lett.,* **4,** 473–476.

Forsyth, D. & Uyeda, S., 1975. On the relative importance of the driving forces of plate motion, *Geophys. J. R. astr. Soc.,* **43,** 163–200.

Gurnis, M., 1989. A reassessment of the heat transport by variable viscosity convection with plates and lids, *Geophys. Res. Lett.,* **16,** 179–182.

Gurnis, M. & Hager, B.H., 1988. Controls of the structure of subducted slabs, *Nature,* **335,** 317–321.

Hager, B.H., 1991. Mantle viscosity: a comparison of models from postglacial rebound and from the geoid, plate driving forces, and advected heat flux, in *Glacial Isostasy, Sea-Level and Mantle Rheology,* pp. 493–513, eds Sabadini, R., Lambeck, K. & Boschi, E., Kluwer, Dordrecht.

Hager, B.H. & O'Connell, R.J., 1979. Kinematic models of large-scale mantle flow, in *J. geophys. Res.,* **84,** 1031–1048.

Hager, B.H. & O'Connell, R.J., 1981. A simple global model of plate dynamics and mantle convection, *J. geophys. Res.,* **86,** 4843–4867.

Hasegawa, A., Horiuchi, S. & Umino, N., 1994. Seismic structure of the northeastern Japan convergent margin: a synthesis, *J. geophys. Res.,* **99,** 22 295–22 311.

Hewitt, J.M., McKenzie, D.P. & Weiss, N.O., 1975. Dissipative heating in convective flows, *J. Fluid Mech.,* **68,** 721–738.

Hirth, G. & Kohlstedt, D.L., 1996. Water in the oceanic upper mantle: implications for rheology, melt extraction and the evolution of the lithosphere, *Earth planet. Sci. Lett.,* **144,** 93–108.

Ho-Liu, P., Hager, B.H. & Raefsky, A., 1987. An improved method of Nusselt number calculations, *Geophys. J. R. astr. Soc.,* **88,** 205–215.

Holland, H.D. & Kasting, J.F., 1992. The environment of the Archean Earth, in *The Proterozoic Biosphere: A Multidisciplinary Study*, pp. 21–24, eds Schopf, W. & Klein, C., Cambridge University Press, Cambridge.

Houseman, G.A. & Gubbins, D., 1997. Deformation of subducted oceanic lithosphere, *Geophys. J. Int.,* **131,** 535–551.

Isacks, B.L. & Barazangi, M., 1977. Geometry of Benioff zones: lateral segmentation and downwards bending of the subducted lithosphere, in *Island Arcs, Deep Sea Trenches and Back-Arc Basins,* pp. 99–114, eds Talwani, M. & Pitman, W.C., AGU, Washington, DC.

Jarrard, R.D., 1986. Relations among subduction parameters, *Rev. Geophys.,* **24,** 217–284.

Karato, S.-I., Paterson, M.S. & Fitzgerald, J.D., 1986. Rheology of synthetic olivine aggregates: influence of grain size and water, *J. geophys. Res.,* **91,** 8151–8176.

Karato, S.–I., Riedel, M.R. & Yuen, D.A., 2000. Structure and deformation of subducted slabs in the transition zone: implications for mantle circulation and deep earthquakes, *Phys. Earth planet. Inter.,* submitted.

Kawakatsu, H., 1986. Double seismic zones: kinematics, *J. geophys. Res.,* **91,** 4811–4825.

King, S.D. & Hager, B.H., 1990. The relationship between plate velocity and trench viscosity in Newtonian and power-law subduction calculations, *Geophys. Res. Lett.,* **17,** 2409–2412.

King, S.D. & Hager, B.H., 1994. Subducted slabs and the geoid, 1, numerical experiments with temperature-dependent viscosity, *J. geophys. Res.,* **99,** 19 843–19 852.

King, S.D., Raefsky, A. & Hager, B.H., 1990. ConMan: vectorizing a finite element code for incompressible two-dimensional convection in the Earth's mantle, *Phys. Earth planet. Inter.,* **59,** 195–207.

Kohlstedt, D.L., Evans, B. & Mackwell, S.J., 1995. Strength of the lithosphere: constraints imposed by laboratory experiments, *J. geophys. Res.,* **100,** 17 587–17 602.

Lenardic, A. & Kaula, W.M., 1994. Self-lubricated mantle convection: two-dimensional models, *Geophys. Res. Lett.,* **21,** 1707–1710.

Lithgow-Bertelloni, C. & Richards, M.A., 1995. Cenozoic plate driving forces, *Geophys. Res. Lett.,* **22,** 1317–1320.

Marquart, G., Schmeling, H. & Braun, A., 1999. Small-scale instabilities below the cooling oceanic lithosphere, *Geophys. J. Int.,* **138,** 655–666.

McKenzie, D., 1969. Speculations on the consequences and causes of plate motions, *Geophys. J. R. astr. Soc.,* **18,** 1–32.

Melosh, H.J. & Raefsky, A., 1980. The dynamical origin of subduction zone topography, *Geophys. J. R. astr. Soc.,* **60,** 333–354.

Moresi, L.-N. & Solomatov, V.S., 1995. Numerical investigations of 2D convection with extremely large viscosity variations, *Phys. Fluids,* **7,** 2154–2162.

Moresi, L.-N. & Solomatov, V.S., 1998. Mantle convection with a brittle lithosphere: thoughts on the global tectonic styles of the Earth and Venus, *Geophys. J. Int.,* **133,** 669–682.

Parmentier, E.M., Turcotte, D.L. & Torrance, K.E., 1976. Studies of finite amplitude non-Newtonian thermal convection with application to convection in the Earth's mantle, *J. geophys. Res.,* **81,** 1839–1846.

Parsons, B. & McKenzie, D., 1978. Mantle convection and the thermal structure of plates, *J. geophys. Res.,* **83,** 4485–4496.

Parsons, B. & Sclater, J.G., 1977. An analysis of the variation of ocean floor bathymetry and heat flow with age, *J. geophys. Res.,* **82,** 803–827.

Ponko, S.C. & Peacock, S.M., 1995. Thermal modeling of the southern Alaska subduction zone: insight into the petrology of the subducting slab and overlying mantle wedge, *J. geophys. Res.,* **100,** 22 117–22 128.

Puster, P., Hager, B.H. & Jordan, T.H., 1995. Mantle convection experiments with evolving plates, *Geophys. Res. Lett.,* **22,** 2223–2226.

Ratcliff, J.T., Tackley, P.J., Schubert, G. & Zebib, A., 1997. Transitions in thermal convection with strongly variable viscosity, *Phys. Earth planet. Inter.,* **102,** 201–212.

Solomatov, V.S., 1995. Scaling of temperature- and stress-dependent viscosity convection, *Phys. Fluids,* **7,** 266–274.

Solomatov, V.S. & Moresi, L.-N., 1996. Stagnant lid convection on Venus, *J. geophys. Res.,* **101,** 4737–4753.

Stein, C.A. & Stein, S., 1992. A model for the global variation in oceanic depth and heat flow with lithospheric age, *Nature,* **359,** 123–129.

Stein, S. & Stein, C.A., 1997. Sea-floor depth and the Lake Wobegon effect, *Science,* **275,** 1613–1614.

Tackley, P.J., 1998. Self-consistent generation of tectonic plates in three-dimensional mantle convection, *Earth planet. Sci. Lett.,* **157,** 9–22.

Toth, J. & Gurnis, M., 1998. Dynamics of subduction initiation at preexisting fault zones, *J. geophys. Res.,* **103,** 18 053–18 067.

Trompert, R. & Hansen, U., 1998. Mantle convection simulations with rheologies that generate plate-like behavior, *Nature,* **395,** 686–689.

Turcotte, D.L. & Oxburgh, E.R., 1967. Finite amplitude convective cells and continental drift, *J. Fluid Mech.,* **28,** 29–42.

Turcotte, D.L. & Schubert, G., 1982. *Geodynamics,* John Wiley, New York.

Zhang, J., Hager, B.H. & Raefsky, A., 1985. A critical assessment of viscous models of trench topography and corner flow, *Geophys. J. R. astr. Soc.,* **83,** 451–475.

Zhong, S. & Gurnis, M., 1994. Controls on trench topography from dynamic models of subducted slabs, *J. geophys. Res.,* **99,** 15 683–15 695.

Zhong, S. & Gurnis, M., 1995a. Mantle convection with plates and mobile, faulted plate margins, *Science,* **267,** 838–843.

Zhong, S. & Gurnis, M., 1995b. Towards a realistic simulation of plate margins in mantle convection, *Geophys. Res. Lett.,* **22,** 981–984.

Zhong, S. & Gurnis, M., 1996. Interaction of weak faults and non-Newtonian rheology produces plate tectonics in a 3D model of mantle flow, *Nature,* **383,** 245–247.

Zhong, S., Gurnis, M. & Moresi, L., 1998. Role of faults, non-linear rheology, and viscosity structure in generating plates from instantaneous mantle flow models, *J. geophys. Res.,* **103,** 15 255–15 268.